ROTATION CALCULATION IN TOKAMAK PLASMA

A Dissertation
Presented to
The Academic Faculty

By

Richard Wendell King III

In Partial Fulfillment
of the Requirements for the Degree
Master of Science in the
Nuclear and Radiological EngineeringProgram

Georgia Institute of Technology

May 2019

ROTATION CALCULATION IN TOKAMAK PLASMA

Approved by:

Dr. Weston M. Stacey Jr., Advisor
School of Nuclear and Radiological Engineering
Georgia Institute of Technology

Dr. Bojan Petrovic
School of Nuclear and Radiological Engineering
Georgia Institute of Technology

Dr. John McCuan
School of Applied Mathematics
Georgia Institute of Technology

Date Approved: April 18, 2019

To my parents,

Reita Mathews King and Dr. Richard Wendell King Jr.,

without whose support, I would have been unable to accomplish this goal.

ACKNOWLEDGEMENTS

I would like to thank Dr. Stacey for his numerous contributions and guidance throughout the course of this project. His contributions are so substantive that they never could really be enumerated. I would also like to thank the committee for their willingness and enthusiasm. Furthermore, this project would have been litter ally impossible to accomplish without the hours upon hours of guidance and instruction I received from Tim Collart. This was supererogatory behavior on Tim's part, having already graduated and having a newborn.

Learning is an integral part of graduate school, as such there are a few instructors which I have not already thanked I would like to thank by name now. I thank Dr. Rahnema for teaching me transport, without which I would have a much shallower understanding of nuclear reactors. I thank Dr. Zhou for explaining nuclear physics in an easy to understand manner. I thank Dr. Yao for influencing my understanding of partial differential equations. I thank Dr. Liu for teaching me numerical methods. I thank Dr. Kang for teaching me approximation theory. I thank Dr. M. Zhou for continuum mechanics. I thank all of the other professors I have had for everything.

Almost as important as intellectual guidance is having a good work environment. For that I would like to give thanks to all of the lab members I have met over the years. So I extend gratitude towards Theresa Wilks, Jonothan Roveto, E. Will DeShazer, Nicolas Piper, and Maxwell Hill. Additionally, the ability to enrich my experience with the perspectives of people from different backgrounds has been of substantial positive influence on my outlook. To that effect, I would like to thank Raffaele Tatali, Dr. Xianwei Wang, and Joel Fossorier. Raffaele deserves a special mention for his providing a very different outlook on life.

Another important aspects to this experience is the set of friends I made along the way. I would like to thank Dingkun Guo, John Norris, William Woolery, and Lars von Wolff for

being good friends.

A special thanks is owed to Lars von Wolff for his help with the mathematics involved. Another thanks is owed to Nick Piper for his help with some of the raw data. Finally a special thanks is owed to Max Hill. In particular for Max's enlightening conversations and eagerness to collaborate.

TABLE OF CONTENTS

LIST OF FIGURES

SUMMARY

Rotation is important in tokamaks because of its effects on confinement and stability. This thesis evaluates the effectiveness of axisymmetric neoclassical gyroviscous theory on determining the toroidal rotation profile in tokamak plasmas. In doing this evaluation, a numerical method for predicting with high accuracy the two-dimensional rotation profiles of a multiple species plasma was developed. This method is of arbitrary precision and is rapidly converging. The organization of this thesis is an introduction to the problem followed by a brief development of axisymmetric neoclassical theory, which omits derivations of neoclassical effects such as particle trapping or gyroviscosity. The third and largest section is dedicated to the development of the numerical method wherein the conforming spectral Galerkin strategy is devised and a streamline potential decomposition of the velocity is formulated. The next section displays the results of our analysis where we show that this axisymmetric neoclassical spectral Galerkin method does indeed predict the toroidal rotation very well in the core and to within a factor of two everywhere. The final section is the conclusion where we discuss the implications of axisymmetric neoclassical theory predicting rotation requires the prediction of poloidal asymmetries.

CHAPTER 1
INTRODUCTION AND BACKGROUND

This thesis evaluates the effectiveness of neoclassical gyroviscous theory on determining the toroidal rotation profile in tokamak plasmas. In the past, it has been observed that neoclassical theory has produced results within an order of magnitude of the experimentally measured data and that each improvement in the geometry and formalism has corresponded to an improvement in the agreement [1, 2, 3, 4, 5, 6, 7, 8, 9]. Our hypothesis then would be that neoclassical transport theory is effective at predicting rotation profiles in tokamak plasmas. We test our hypothesis by implementing a numerical code which evaluates the rotation that would be found if gyroviscosity is the dominant rotation damping mechanism and compare that predicted profile with an experimentally fit profile.

1.1 Significance

Fusion is the process by which two light nuclei combine to form a heavier nucleus [10]. For example in a star, four hydrogen atoms (H^1) fuse, through multiple events, to create a net gain of one helium atom [11]. The resultant atom will be in an excited state and almost immediately decay into two other nuclei [10]. This process can release a massive amount of energy carried by the resultants in the form of kinetic energy [11]. For the past 70 years, it has been thought that if humanity could harvest the power of fusion, then the process by which this was accomplished would be a source of essentially infinite free energy [12]. This lead to a major scientific and engineering interest in the development of a fusion reactor [10]. The largest international developments have been spearheaded by the International Thermonuclear Experimental Reactor (ITER) [10].

Fusion requires a high speed of collision in order to make the reaction probable [11]. In order to have these high speeds, high temperatures become necessary; fusion as a result

of high temperatures is thus called *thermonuclear fusion* [11]. These high temperatures naturally lead to a reactor characterized by having plasma fuel. One of the early primary technical challenges was the design and manufacture of a device which could contain a thermonuclear plasma. To date, the most successful solution to the problem of containing plasma is a *tokamak* [10].

Tokamaks are fusion devices in which a toroidal magnetic field traps particles at high temperatures in order to confine a plasma undergoing favorable conditions for fusion. If a charged particle is moving in a magnetic field, it will *gyrate*, moving in a centered circle, around a magnetic field line due to the Lorentz force. Conceptually, this means that a charged particle can be kept within the vicinity of a 3-dimensional curve no matter how fast the particle is traveling; therefore, if the magnetic fields can be flattened on a surface, then no particle should be able to escape that surface. Due to a fundamental theorem in topology, any magnetic confinement device must have a hole in order to work [13]. For this reason, topologically, a tokamak can be considered a torus.

In a tokamak, *toroidal rotation*, the bulk movement of the plasma in the toroidal direction, stabilizes against magnetohydrodynamic (MHD) instabilities, is important to resistive wall tearing (RWT), can play pivotal roles in shear flows and turbulence suppression, and is key for confinement [14, 10].

It is important for the continued development and improvement of steady thermonuclear devices to calculate toroidal rotation accurately. Braginskii developed the viscosity tensor in Cartesian coordinates with z being the magnetic direction for a collisional plasma [15]. Later the formulae for neoclassical viscosity tensors in toroidal axisymmetric flux surface geometry were developed [1] and extended to arbitrary collisionallity [2]. To that effect, the extended gyroviscous model has been used in the past with some success [6, 9]. In this model the gyroviscosity is the leading order viscous effect in the toroidal momentum balance; therefore, as will become apparent in chapter 2, this model depends heavily upon poloidal asymmetries of geometry, velocity, and density to calculate the toroidal gyrovis-

cosity and rotation velocity. Previous versions of this model have predicted the toroidal rotation within a factor of two in the core where the assumption of toroidal axisymmetry should be adequate, but they provided much less accurate calculations of the toroidal rotation in the vicinity of the edge plasma where the assumption of toroidal axisymmetry is more questionable [16].

1.2 Novelty

The thesis goal of evaluating the effectiveness of axisymmetric neoclassical theory when implemented in two dimensions is also novel for a few reasons. Before explaining how the theory is novel we explain why a precise evaluation of axisymmetric neoclassical theory must be two dimensional in order to really capture the physics.

Neoclassical theory is a theory of plasma transport that takes into account the effects of toroidal geometry [17]. The formulae for neoclassical viscosity tensors were first extended to toroidal flux surface geometry in 1985 [1]. Using these formulae and performing a *flux surface average* (FSA), which is defined in the appendix, the contribution to the FSA of the toroidal viscous stress of the "parallel" viscosity component is identically zero. The other two components of the FSA of the viscous stress are the perpendicular viscosity and gyroviscosity components. The gyroviscosity has a coefficient that is three orders of magnitude larger than the perpendicular viscosity coefficient. This axisymmetric neoclassical model has predicted central toroidal rotation within an order of magnitude of experiment [3, 5] using a circular flux surface model ($B(r,\theta) = \frac{B_0(r)}{1+\frac{r}{R}\cos(\theta)}$). In those early calculations, the flux circular surface model and lowest order Fourier expansion were used to calculate poloidal asymmetries that determine the magnitude of the Braginskii toroidal gyroviscosity. The equations were later cast in a form usable with a more poloidally asymmetric [18] Miller Flux equilibrium [19]. Refinement of the poloidal asymmetry calculation using a Miller model flux surface led to an order of magnitude improvement in agreement with experimental toroidal velocity in the central region of DIII-D [6]. This led to the creation

of an iterative code for a first order poloidal Fourier decomposition, GTROTA [7]. An orthogonalized flux-surface aligned localized coordinate frame [9] has been developed to improve calculations of poloidal asymmetries.

In this thesis, the model is extended in order to calculate poloidal asymmetries and velocities to evaluate how well an accurate calculation of the extended Braginskii gyroviscosity can describe the toroidal momentum damping in the central regions of DIII-D. We have extended the applicability of this model to the plasma edge region, where the effects of asymmetries are more pronounced. There are two fundamental difference between the calculations in this thesis and ones in the past. In the past, a separation of variables assumption and lowest order Fourier series approximation was used. In the present model, the full set of 2D partial differential equations are solved using a weak formulation with a higher order Bessel-Fourier expansion.

1.3 Purpose and Organization of Thesis

The difficulty of obtaining agreement between theory and experiment has led to the hypothesis that most transport in a plasma is of an anomalous origin, leading to task forces to determine the nature of this transport [20]. The anomalous theory is mostly ad-hoc or based on arguments such as [21] that transport should be diffusive in nature. The more robust theory of transport is "neoclassical" transport. The purpose of this thesis is to rigorously calculate if axisymmetric neoclassical transport is the dominant effect in determining the toroidal rotation in a tokamak.

The organization of this thesis is as follows: in chapter two we develop the axisymmetric neoclassical theory whose rigorous application is this thesis' goal; in chapter three we discuss our solution method for the equations derived from the model presented in axisymmetric neoclassical theory through elaboration of the numerical method used as well as the explanation of a novel decomposition of the vector field into three scalar fields to create a conforming spectral element model. The fourth chapter is where we display the

results of the analysis to test the effectiveness of pure axisymmetric neoclassical theory in determining plasma rotation. We conclude with the fifth chapter where we discuss future challenges and implications of these results presented in this thesis.

CHAPTER 2

NEOCLASSICAL THEORY: A MULTI-FLUID APPROACH TO PLASMA TRANSPORT

We have established the evaluation of how well axisymmetric neoclassical theory can account for toroidal rotation in plasma as our goal in this thesis. In order to carry out this evaluation, we must first define what we mean by neoclassical theory; accordingly, in this chapter, we formulate the equations that we use to model the rotation in a plasma. The practical fact is that plasma is a collection of charged particles behaving in a primarily Newtonian physics manner. This means that the Boltzmann equation describes the evolution of the distribution function with high accuracy; therefore, the essential background is that we will actualize the fundamental equations used for the modeling of plasma and then particularize the closure relationships employed to make them solvable.

2.1 Plasma Fluid Equations

The approach used in this analysis is known as plasma multifluid theory. The fluid equations are derived from the Boltzmann equation. The Boltzmann transport equation (BTE), equation (2.1) describes the evolution of a particle distribution over time in the presence of external forces, inter-particle collisions, and sources/sinks of particles [10].

$$\frac{\partial f_\sigma}{\partial t} + \boldsymbol{v}_\sigma \cdot \frac{\partial f_\sigma}{\partial \boldsymbol{x}_\sigma} + \frac{e_\sigma}{m_\sigma} \left(\boldsymbol{E} + \boldsymbol{v}_\sigma \times \boldsymbol{B} \right) \cdot \frac{\partial f_\sigma}{\partial \boldsymbol{v}_\sigma} = S_\sigma + \sum_{\sigma'} C_{\sigma\sigma'}(f_\sigma, f_{\sigma'}) \tag{2.1}$$

In this equation:

- σ and σ' represents a particle species such as deuterium, tritium, etc.,
- t is the time variable,

- $\boldsymbol{x}$ represents position in three dimensional space,
- $\boldsymbol{v}$ represents velocity in three dimensional space,
- f represents the particle density function as a function of space velocity and time,
- e represents the charge of a particle,
- m represents the mass of a particle,
- S represents the volumetric space-velocity source density (how many particles are generate at a point $\boldsymbol{x} = (x, y, z)$ with velocity $\boldsymbol{v} = (v_x, v_y, v_z)$ per second),
- $C_{\sigma\sigma'}(f_\sigma, f_{\sigma'})$ represents the volumetric space-velocity effect density of collisions between the two entire distributions f_σ and $f_{\sigma'}$ on the rate of change of f_σ,
- $\boldsymbol{E}$ is the electric field,
- $\boldsymbol{B}$ is the magnetic flux density (magnetic field), and
- $\times$, $\cdot$, and ∂ all have their standard meanings.

The perhaps unusual aspect of the notation is best explained in Cartesian coordinates:

$$\boldsymbol{v} \cdot \frac{\partial f(t, \boldsymbol{x}, \boldsymbol{v})}{\partial \boldsymbol{x}} = v_x \frac{\partial f(t, x, y, z, v_x, v_y, v_z)}{\partial x} + v_y \frac{\partial f(t, x, y, z, v_x, v_y, v_z)}{\partial y} + v_z \frac{\partial f(t, x, y, z, v_x, v_y, v_z)}{\partial z} \quad (2.2)$$

To obtain the fluid equations, we first multiply the BTE by a weighing function, z, called a *velocity moment*. We then integrate the BTE over velocity space as shown bellow to obtain a system of partial differential equations (PDEs).

$$\int \mathrm{d}\boldsymbol{v} z_n \left(\frac{\partial f_\sigma}{\partial t} + \boldsymbol{v}_\sigma \bullet \frac{\partial f_\sigma}{\partial \boldsymbol{x}_\sigma} + \frac{e_\sigma}{m} (\boldsymbol{E} + \boldsymbol{v}_\sigma \times \boldsymbol{B}) \bullet \frac{\partial f_\sigma}{\partial \boldsymbol{v}_\sigma} \right) = C_\sigma^n + S_\sigma^n \quad (2.3)$$

Where $C_\sigma^n = \int \mathrm{d}\boldsymbol{v} z_n \sum_{\sigma'} C_{\sigma\sigma'}(f_\sigma, f_{\sigma'})$ and $S_\sigma^n = \int \mathrm{d}\boldsymbol{v} z_n S_\sigma$. We have used the following expressions for z_n:

$$z_0 = 1, \tag{2.4}$$

$$z_1 = m\boldsymbol{v}, \tag{2.5}$$

$$z_2 = \frac{1}{2} m \left(\boldsymbol{v} \bullet \boldsymbol{v}\right), \tag{2.6}$$

$$z_3 = \frac{1}{2} m \left(\boldsymbol{v} \bullet \boldsymbol{v}\right) \boldsymbol{v}. \tag{2.7}$$

Performing this integration results in the following four moments-equations [10]. The continuity equation is given by equation (2.8). The momentum balance equation is given by equation (2.9). The energy balance equation is given by equation (2.10). The energy flux equation is given by equation (2.11).

$$\frac{\partial n_\sigma}{\partial t} + \nabla \bullet \left(n_\sigma \boldsymbol{v}_\sigma\right) = S_\sigma^0. \tag{2.8}$$

$$m_\sigma \frac{\partial n_\sigma \boldsymbol{v}_\sigma}{\partial t} + \boldsymbol{\nabla} \bullet \boldsymbol{M}_\sigma - n_\sigma e_\sigma \left(\boldsymbol{E} + \boldsymbol{v}_\sigma \times \boldsymbol{B}\right) = \boldsymbol{R}_\sigma^1 + \boldsymbol{S}_\sigma^1. \tag{2.9}$$

$$\frac{1}{2} \frac{\partial \mathrm{Tr}\left[\boldsymbol{M}_\sigma\right]}{\partial t} + \nabla \bullet \boldsymbol{Q}_\sigma = n_\sigma e_\sigma \boldsymbol{v}_\sigma \bullet \boldsymbol{E} + R_\sigma^2 + S_\sigma^2. \tag{2.10}$$

$$\frac{\partial \boldsymbol{Q}_\sigma}{\partial t} + \boldsymbol{\nabla} \bullet \boldsymbol{\theta}_\sigma - \frac{1}{2} \frac{e_\sigma}{m_\sigma} \mathrm{Tr}\left[\boldsymbol{M}_\sigma\right] \boldsymbol{E} - \frac{e_\sigma}{m_\sigma} \boldsymbol{M}_\sigma \bullet \boldsymbol{E} - \frac{e_\sigma}{m_\sigma} \boldsymbol{Q}_\sigma \times \boldsymbol{B} = \boldsymbol{R}_\sigma^3 + \boldsymbol{S}_\sigma^3. \tag{2.11}$$

These equations can be infinitely expanded, and they require closure and constituent relationships. The terms are defined as follows [10].

- n_σ is the number density of the species,

- $\nabla\bullet$ represents the divergence operator,
- $\boldsymbol{\nabla}\bullet$ represent the tensor divergence operator,
- S_σ^0 represent the source of particle with species σ,
- $\boldsymbol{M}_\sigma$ is the momentum stress tensor,
- $\boldsymbol{R}_\sigma^1$ is the first collisional friction,
- $\boldsymbol{S}_\sigma^1$ is the momentum source,
- Tr $[\boldsymbol{M}_\sigma]$ is the scalar trace of the momentum stress tensor,
- $\boldsymbol{Q}_\sigma$ is the energy flow vector,
- R_σ^2 is the second collisional friction,
- S_σ^2 is the energy source,
- $\boldsymbol{\theta}_\sigma$ is the energy flux tensor,
- $\boldsymbol{R}_\sigma^3$ is the third collisional friction, and
- $\boldsymbol{S}_\sigma^3$ is the energy flux source vector.

For our purposes, we examine only the first two moments equations, the momentum and continuity equations. Before continuing onward, we need to discuss the momentum stress tensor in some detail.

2.1.1 Momentum Stress Tensor

The momentum stress tensor is the dominant damping term in the momentum equations. Typically, we begin by a change of variables of the velocity term in the Boltzmann equation as shown bellow.

$$\boldsymbol{v} = \boldsymbol{v}_\sigma + \boldsymbol{W} \tag{2.12}$$

Here, $\boldsymbol{v}$ is the true velocity; $\boldsymbol{v}_\sigma$ is the fluid velocity, and $\boldsymbol{W}$ is the new variable of which we write the distribution. The fluid velocity is defined as:

$$\begin{aligned}\boldsymbol{v}_\sigma &\equiv \frac{\int f_\sigma(\boldsymbol{v})\boldsymbol{v}\mathrm{d}^3\boldsymbol{v}}{\int f_\sigma(\boldsymbol{v})\mathrm{d}^3\boldsymbol{v}} \\ &\equiv \frac{\int f_\sigma(\boldsymbol{v})\boldsymbol{v}\mathrm{d}^3\boldsymbol{v}}{n_\sigma}\end{aligned} \tag{2.13}$$

Using change of variables, we can prove the following property [10]:

$$\begin{aligned}\int f_\sigma(\boldsymbol{W})\boldsymbol{W}\mathrm{d}^3\boldsymbol{W} &= \int f_\sigma(\boldsymbol{v})\left(\boldsymbol{v}-\boldsymbol{v}_\sigma\right)\mathrm{d}^3\boldsymbol{v} \\ &= \int f_\sigma(\boldsymbol{W})\boldsymbol{v}\mathrm{d}^3\boldsymbol{v} - \boldsymbol{v}_\sigma\int f_\sigma(\boldsymbol{W})\mathrm{d}^3\boldsymbol{v} \\ &= n_\sigma\boldsymbol{v}_\sigma - n_\sigma\boldsymbol{v}_\sigma \\ &= 0.\end{aligned} \tag{2.14}$$

Therefore, we can rewrite the momentum stress tensor as:

$$\boldsymbol{M}_\sigma = n_\sigma m_\sigma \boldsymbol{v}_\sigma\boldsymbol{v}_\sigma + \boldsymbol{P}_\sigma. \tag{2.15}$$

We define:

$$\boldsymbol{P}_\sigma \equiv n_\sigma m_\sigma(\boldsymbol{W}\boldsymbol{W})_\sigma = m_\sigma\int f_\sigma(\boldsymbol{v})\boldsymbol{W}\boldsymbol{W}\mathrm{d}^3\boldsymbol{v}. \tag{2.16}$$

We decompose this into an isotropic and anisotropic pressure.

$$\boldsymbol{P} = \frac{1}{3}(\mathrm{Tr}\left[\boldsymbol{P}_\sigma\right])\boldsymbol{I} + \boldsymbol{\Pi}_\sigma \tag{2.17}$$

We also call $\boldsymbol{\Pi}_\sigma$ the *viscosity tensor*. A deeper theory is known as the Fokker–Planck theory [22] and the drift–kinetic theory [23] comes into play for calculation of this anisotropic

tensor.

Braginskii [24, 15] developed the first rigorous treatment of viscosity in the context of collisional plasma fluid theory. He developed an improved way of decomposing the viscosity tensor into physically meaningful components and calculating those components in a collisional plasma.

2.2 Braginskii Closure of Fluid Equations

There have been several ways to provide a complete system of equations for equations (2.8) through (2.11) [25, 26, 21]. One such method was developed by Braginskii [15] where he considered three different components of particle movement in a constant magnetic field. The first is the *parallel* component, represented by $\|$, which is the movement of a particle in the direction of the magnetic field. The second is the *gyromotional* component, represented by Ω, which is the movement of a particle around the field lines. The third component is the *perpendicular* component, represented by $\perp$, which is the movement of a particle perpendicular to the magnetic field.

Braginskii [24, 15] calculated the transport coefficients using the Laguerre polynomials' generator function. To facilitate the calculation, Braginskii used an approximate form of the collisional forces and a similar approximation for ion-electron collisions [24]. As an additional simplification, Braginskii perturbs the Maxwellian as $f(x,v) = f_0(x,v)(1 + \phi(x,v))$ and treats collisions as a perturbation to the Boltzmann equation rather than using some generalized perturbation.

By performing the calculation, he obtains the viscosity coefficients by solving for ϕ in

$$C(f_0, f_0\phi) + C(f_0\phi, f_0) + f_0 v \times B\nabla_v\phi = s_{ik}w_{ik}$$

where $C(a,b)$ is the Coulomb collision integral. By splitting the above equation into three orthogonal equations, Braginskii obtained some of the viscosity coefficients that are used

in this analysis.

Braginskii's uses five viscosity coefficients [15]. These coefficients are for deuterium [15]:

$$\eta_0 = 0.96\ nT\tau \tag{2.18}$$

$$\eta_1 = nT\tau \frac{4.8\ \Omega^2\tau^2 + 2.23}{16\ \Omega^4\tau^4 + 8.12\ \Omega^2\tau^2 + 2.33} \tag{2.19}$$

$$\eta_2 = nT\tau \frac{1.2\ \Omega^2\tau^2 + 2.23}{\Omega^4\tau^4 + 2.03\ \Omega^2\tau^2 + 2.33} \tag{2.20}$$

$$\eta_3 = 2nT\Omega\tau^2 \frac{4\ \Omega^2\tau^2 + 2.38}{16\ \Omega^4\tau^4 + 8.12\ \Omega^2\tau^2 + 2.33} \tag{2.21}$$

$$\eta_4 = nT\Omega\tau^2 \frac{\Omega^2\tau^2 + 2.38}{\Omega^4\tau^4 + 2.03\ \Omega^2\tau^2 + 2.33} \tag{2.22}$$

Where T is temperature, Ω is the gyrofrequency, and τ is the collision time.

$$\Omega = \frac{e\|\boldsymbol{B}\|}{m} \tag{2.23}$$

It is easy to see that in the limit as gyrofrequency approaches infinity, we are left with the more popular Braginskii viscosity coefficients [15]:

$$\eta_0 = 0.96\ nT\tau \tag{2.24}$$

$$\eta_1 = \frac{3}{10}\frac{nT}{\Omega^2\tau} \tag{2.25}$$

$$\eta_2 = \frac{12}{10}\frac{nT}{\Omega^2\tau} \tag{2.26}$$

$$\eta_3 = \frac{1}{2}\frac{nT}{\Omega} \tag{2.27}$$

$$\eta_4 = \frac{nT}{\Omega} \tag{2.28}$$

The constituent relation for a stress measure must be objective [27]. Hooke's law is one of the simplest stress closures. The general form for an object is related to Hooke's law [27]. Equation (2.29) gives a general expression for Hooke's law using Einstein summation

convention.

$$\Pi^{ij} = C^{ij}_{kl} W^{kl} \tag{2.29}$$

Where W is the rate of strain tensor. Braginskii decomposed the viscosity tensor into five orthogonal components [15].

$$\mathbf{\Pi} = \mathbf{\Pi}_{\parallel} + \mathbf{\Pi}_{\perp} + \mathbf{\Pi}_{\Omega} = \mathbf{\Pi}^{ij}_0 + (\mathbf{\Pi}^{ij}_1 + \mathbf{\Pi}^{ij}_2) + (\mathbf{\Pi}^{ij}_3 + \mathbf{\Pi}^{ij}_4) \tag{2.30}$$

He however did this in Cartesian coordinates. Later on Stacey and Sigmar worked out the tensor in toroidal coordinates [1]. This yields the following expressions for the flux surface average:

$$\left\langle R^2 \nabla\phi \cdot \nabla \cdot \mathbf{\Pi} \right\rangle = \left\langle R^2 \nabla\phi \cdot \nabla \cdot \mathbf{\Pi}_{\perp} \right\rangle + \left\langle R^2 \nabla\phi \cdot \nabla \cdot \mathbf{\Pi}_{\Omega} \right\rangle \tag{2.31}$$

Where,

$$\left\langle R^2 \nabla\phi \cdot \nabla \cdot \mathbf{\Pi}_{\Omega} \right\rangle = -\left\langle \frac{1}{R h_p} \frac{\partial}{\partial l_\psi} \left(R^3 h_p \eta_4 \frac{\partial}{\partial l_p} \left(\frac{v_\phi}{R} \right) \right) \right\rangle \tag{2.32}$$

$$\left\langle R^2 \nabla\phi \cdot \nabla \cdot \mathbf{\Pi}_{\perp} \right\rangle = -\left\langle \frac{1}{R h_p} \frac{\partial}{\partial l_\psi} \left(R^3 h_p \eta_2 \frac{\partial}{\partial l_\psi} \left(\frac{v_\phi}{R} \right) \right) \right\rangle \tag{2.33}$$

The following equations show the viscous tensors worked out in an orthogonal geometry [28]:

$$\pi_0 = -3\eta_0 \left(\boldsymbol{b} \otimes \boldsymbol{b} - \frac{1}{3}\boldsymbol{I} \right) \left(\boldsymbol{b} \otimes \boldsymbol{b} - \frac{1}{3}\boldsymbol{I} \right) : \nabla V \tag{2.34}$$

$$\pi_1 = -\eta_1 \left[\boldsymbol{I}_{\perp} \cdot \boldsymbol{W} \bullet \boldsymbol{I}_{\perp} + \frac{1}{2}\boldsymbol{I}_{\perp}(b \bullet \boldsymbol{W} \bullet b) \right] \tag{2.35}$$

$$\pi_2 = -4\eta_1 \left[\boldsymbol{I}_{\perp} \cdot \boldsymbol{W} \bullet \boldsymbol{b} \otimes \boldsymbol{b} + \boldsymbol{b} \otimes \boldsymbol{b} \cdot \boldsymbol{W} \cdot \boldsymbol{I}_{\perp} \right] \tag{2.36}$$

$$\pi_3 = \frac{\eta_3}{2} \left[\boldsymbol{b} \times \boldsymbol{W} \cdot \boldsymbol{I}_{\perp} - \boldsymbol{I}_{\perp} \cdot \boldsymbol{W} \times \boldsymbol{b} \right] \tag{2.37}$$

$$\pi_4 = 2\eta_3 \left[\boldsymbol{b} \times \boldsymbol{W} \cdot \boldsymbol{b} \otimes \boldsymbol{b} - \boldsymbol{b} \otimes \boldsymbol{b} \cdot \boldsymbol{W} \times \boldsymbol{b} \right] \tag{2.38}$$

Where $\boldsymbol{b}$ is a unit vector parallel to the magnetic field, and η represents a viscosity coefficient. This formula inherently assumes an orthonormal frame. To do this more generally, let $(f^1, f^2, f^3) = \boldsymbol{b}$, and define

$$\perp^{\alpha\beta} = g^{\alpha\beta} - f^\alpha f^\beta \tag{2.39}$$

Where g is the metric tensor. Then we obtain

$$\pi_0^{\alpha\beta} = -\frac{3}{2}\eta_0 \left(f^\alpha f^\beta - \frac{1}{3} g^{\alpha\beta} \right) \left(f_\mu f_\nu - \frac{1}{3} g_{\mu\nu} \right) W^{\mu\nu} \tag{2.40}$$

$$\pi_1^{\alpha\beta} = -\eta_1 \left[\perp_\mu^\alpha \perp_\nu^\beta + \frac{1}{2} \perp^{\alpha\beta} f_\mu f_\nu \right] W^{\mu\nu} \tag{2.41}$$

$$\pi_2^{\alpha\beta} = -4\eta_1 \left[\perp_\mu^\alpha f^\beta f_\nu + f^\alpha \perp_\nu^\beta f_\mu \right] W^{\mu\nu} \tag{2.42}$$

$$\pi_3^{\alpha\beta} = \frac{\eta_3}{2} \left[\xi^{\alpha\gamma\zeta} g_{\zeta\mu} \perp_\nu^\beta + \perp_\nu^\alpha \xi^{\beta\gamma\zeta} g_{\zeta\nu} \right] f_\gamma W^{\mu\nu} \tag{2.43}$$

$$\pi_4^{\alpha\beta} = 2\eta_3 \left[\xi^{\alpha\gamma\zeta} g_{\zeta\mu} f^\beta f_\nu + f^\alpha f_\mu \xi^{\beta\gamma\zeta} g_{\zeta\nu} \right] f_\gamma W^{\mu\nu} \tag{2.44}$$

Where ξ is the Levi-Civita symbol. These are the formula that we use for our viscosity representation.

Shaing, Sigmar, and Stacey give the formula for the axisymmetric neoclassical parallel viscosity as [2]:

$$\eta_{0j} = \frac{n_j m_j q^2 R^2 \nu_{jj}}{\left(\epsilon \frac{3}{2} + \frac{qR\nu_{jj}}{v_{th}} \right) \left(1 + \frac{qR\nu_{jj}}{v_{th}} \right)} \tag{2.45}$$

Here, q is the safety factor; R is the major radius; ϵ is the aspect ratio; v_{th} is the thermal velocity, and ν_{jj} is the self collision frequency. The other two coefficients are given as

$$\eta_{1j} = \frac{3n_j T_j \nu_{jj}}{10\Omega_j^2} \tag{2.46}$$

$$\eta_{3j} = \frac{n_j T_j}{2\Omega_j} \tag{2.47}$$

From this, we see that

$$\eta_0 >> \eta_3 >> \eta_1 \tag{2.48}$$

Hence, the perpendicular viscosity is much less than the gyroviscosity and even smaller than the parallel viscosity.

2.3 Used Multi-Fluid Equations

Previous calculations [5, 6] based upon the Braginskii [15] gyroviscous tensor with an assumed Miller flux surface geometry [18], over-predicted the toroidal rotation by a factor of 2 or less in the core, but by more in the edge.

The aforementioned plasma multifluid equations are useful for simulations of plasmas. The first two standard multifluid equations are [10]:

$$\frac{\partial n_\sigma}{\partial t} + \nabla \cdot (n_\sigma \boldsymbol{v}_\sigma) = S_\sigma^0. \tag{2.49}$$

$$m_\sigma \frac{\partial n_\sigma \boldsymbol{v}_\sigma}{\partial t} + \nabla \cdot \mathbf{M}_\sigma - n_\sigma e_\sigma \left(\boldsymbol{E} + \boldsymbol{v}_\sigma \times \boldsymbol{B}\right) = \boldsymbol{R}_\sigma^1 + \boldsymbol{S}_\sigma^1. \tag{2.50}$$

Where each equation is species–specific.

In component form, the momentum equation becomes

$$m_\sigma \frac{\partial n_\sigma v_\sigma^i}{\partial t} + \nabla_j n_\sigma m_\sigma v_\sigma^i v_\sigma^j + \nabla^i p_\sigma + \nabla_j \Pi_\sigma^{ij} - n_\sigma e_\sigma E^i + n_\sigma e_\sigma v_\sigma^k B^l \xi_{\cdot kl}^i = \sum \nu_{\sigma,\sigma'} \left(m_\sigma n_\sigma v_\sigma^i - m_{\sigma'} n_{\sigma'} v_{\sigma'}^i \right) + S_{\sigma 1}^i \quad (2.51)$$

where, using Einstein summation notation:

$$\Pi^{ij} = \Pi_\parallel^{ij} + \Pi_\perp^{ij} + \Pi_\Omega^{ij} = \pi_0^{ij} + (\pi_1^{ij} + \pi_2^{ij}) + (\pi_3^{ij} + \pi_4^{ij}) \quad (2.52)$$

$$b^i = \frac{B^i}{\sqrt{g_{jk} B^j B^k}} \quad (2.53)$$

$$\perp^{ij} = g^{ij} - b^i b^j \quad (2.54)$$

$$W^{ij} = \nabla^i v^j + \nabla^j v^i - \frac{2}{3} g^{ij} \nabla_k v^k \quad (2.55)$$

$$\pi_0^{ij} = -3\eta_0 \left(b^i b^j - \frac{1}{3} g^{ij} \right) \left(b^k b^l - \frac{1}{3} g^{kl} \right) g_{lm} \nabla_k v^m \quad (2.56)$$

All other formulas are the same as before. As an important note, we keep density as a scalar field of weight 0, meaning that the volume weights are kept in the differential volume term during volume integrals rather than in variables [29].

2.4 Geometry

As previously mentioned, neoclassical theory takes into account the geometry of a plasma [17]. When we talk about the geometry of a plasma, we are referring to the geometry of the

flux surfaces. Flux surfaces are surfaces that are everywhere tangent to the magnetic field. A more detailed discussion on flux surfaces is in the appendix. For us, the flux surfaces give the magnetic fields and describe the natural coordinate system to perform calculations.

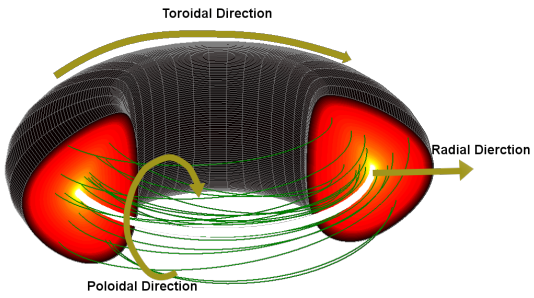

Figure 2.1: The geometry of a tokamak plasma.

We use the Miller [18] coordinate system to perform this calculation. Specifically, we use a normalized, (poloidally) asymmetric Miller model [9] where the radius term varies from 0 to 1.

$$R(\rho,\theta) = R_0(\rho) + a\rho\cos\left(\theta + \left(\sin^{-1}\delta\right)\sin\theta\right) \tag{2.57}$$

$$Z(\rho,\theta) = a\kappa(\rho)\rho\sin\theta \tag{2.58}$$

Here, we have used

- R is major radius in cylindrical coordinates,
- Z is height in cylindrical coordinates,
- ρ is normalized minor radius,
- θ is the poloidal angle,
- κ is the elongation,
- a is the minor radius at $\rho = 1$,

- R_0 is the center of the surface, and
- δ is the triangularity.

The elongation and triangularity are different on the top and bottom for a tokamak. The asymmetry in this model refers to using a different value in the top and bottom to account for that. Each of these terms has a geometric meaning as well. The minor radius gives the width of the plasma. The elongation gives the ratio of the width to the height of a plasma. The triangularity determines how far shifted the major radius at the highest point of a surface is from R_0.

In order to keep the system right handed, we have to say that we are transforming from (R, Z, ϕ) into (ρ, θ, ϕ). This numbering leads to a clockwise toroidal coordinate. The directions of each of the coordinates is shown in figure 2.1. The magnetic field generated from this geometry is given by equation (2.59) [18].

$$B_p = |\nabla\phi \times \nabla\psi(\rho)| \tag{2.59}$$

Where ϕ is the toroidal angle and $\psi(\rho)$ is the magnetic flux. The magnetic flux is only a function of minor radius in the coordinate system used. This is one of the primary advantages of this coordinate system.

2.5 Concluding Remarks

In the next chapter we will use numerical techniques to discretize and solve a system of eight PDEs from the following four equations:

$$\partial_t n_d + \nabla \bullet n_d \boldsymbol{v_d} = S_d^0. \tag{2.60}$$

$$\partial_t \boldsymbol{v_d} + \boldsymbol{v_d} \cdot \boldsymbol{\nabla} \boldsymbol{v_d} + \frac{\nabla p_d}{m_d n_d} + \frac{\boldsymbol{\nabla} \bullet \boldsymbol{\pi_d}}{n_d m_d} = \frac{\boldsymbol{S_d^1}}{n_d m_d} + \frac{e_d}{m_d}\boldsymbol{E} + \frac{e_d}{m_d}\boldsymbol{v_d} \times \boldsymbol{B} + \frac{\nu_{dc}}{m_d}(\boldsymbol{v_c} - \boldsymbol{v_d}) - \frac{S_d^0 \boldsymbol{v_d}}{n_d}. \tag{2.61}$$

$$\partial_t n_c + \nabla \bullet n_c \boldsymbol{v_c} = 0. \tag{2.62}$$

$$\partial_t \boldsymbol{v_c} + \boldsymbol{v_c} \cdot \boldsymbol{\nabla} \boldsymbol{v_c} + \frac{\nabla p_c}{m_c n_c} + \frac{\boldsymbol{\nabla} \bullet \boldsymbol{\pi_c}}{n_c m_c} = \frac{e_c}{m_c}\boldsymbol{E} + \frac{e_c}{m_c}\boldsymbol{v_c} \times \boldsymbol{B} + \frac{\nu_{cd}}{m_c}(\boldsymbol{v_d} - \boldsymbol{v_c}). \tag{2.63}$$

Where equation (2.60) is the deuterium continuity equation, equation (2.61) is the deuterium momentum conservation equation; equation (2.62) is the carbon continuity equation, and equation (2.63) is the carbon conservation of momentum equation.

CHAPTER 3

SOLUTION TO THE ROTATION PROBLEM BASED ON NEOCLASSICAL THEORY: DEVELOPMENT OF A CODE

In the previous chapter, we derived and explained the equations whose solution would allow us to evaluate the primary question of this thesis; specifically, we obtained a set of four equations that represent the "neoclassical" theory of plasma transport. The solution to those equations produces a toroidal rotation velocity profile, which could be scrutinized against the experimental toroidal velocity to illuminate *how well neoclassical theory characterizes transport*.

In this chapter, we introduce and expatiate upon a method to establish an approximate solution to equations (2.60) through (2.63). To that effect, numerical methods are required in order to find an approximate solution. There are three main ways to discretize partial differential equations for solving with a computer: the first and most popular is the finite difference method. The second and most used for computational fluid dynamics is the finite volume method. The last and most flexible is the Galerkin method. The Galerkin method works by taking integrals of the system of equations with respect to test functions to solve a so-called *weak formulation* of the PDEs, which leads to a discretization that is as flexible and general as desired. The most common Galerkin method is the finite element method. This corresponds to using piecewise test functions with "compact support" which is to say function which are non-zero on only a small part of the domain. We use the spectral element or spectral Galerkin method, which simply means our functions have global support (non-zero almost everywhere).

This chapter represents the biggest departure from all previous work. In the past, it has been assumed that the separation of variables could be used for the solution to the equations [4]. Additionally, we have not updated our derivative values directly, instead working in

a "gradient scale length" formalism [7]. We now remove those assumptions and update all or derivatives and solve the equations to arbitrary precision using our library [30]. The difference between the model presented here and models in the rest of the field is that we use the axisymmetric neoclassical correct Shaing-Sigmar-Stacey [2] parallel viscosity instead of the classical one used by codes like NIMROD [31]. Another key difference is that we use the actual fluid equations unlike codes such as UEDGE which use an approximate form. A key difference still between GTROTA and this model is the use of more correct calculus operators [9] in this model. Finally, we do not use any anomalous transport model.

The organization of this chapter is as follows: we discuss the actual equations used for the discretization including approximations and numerical stabilization terms; then we provide an overview of the finite element theory for convective problems; we write the finite element formula we use; we discuss our discretization; finally, we discuss our advancement to steady state technique.

3.1 Numerical Equations

In order to obtain a stable solution to our problem, a number of approximations and stabilization terms are required. The equations we are using are nearly *hyperbolic* (see Appendix). Typically for hyperbolic problems, very special methods of solution are required which must be proven to obtain the same result as the actual system would analytically. There are many such methods [32, 33]; however, they all require solutions to Riemann problems. To avoid this complexity, there are methods, such as the Lax–Friedrichs method, which add in an amount of diffusion required to have a stable system without using one-sided methods or flux solvers [34]. In order to have a stable even order discretization, a parabolic or elliptic equation is required [35]. It is also known that for any odd order approximation to a hyperbolic system, there exists a parabolic PDE whose even order approximation yields the same numerical solution. As a simple example, consider Burger's

equation (3.1).

$$u_t + uu_x = 0 \tag{3.1}$$

Where u is the variable being solved for. With initial conditions:

$$u(x,0) = \begin{cases} 1 & x < .5 \\ 0 & x > .5 \end{cases} \tag{3.2}$$

This solution will have a propagating shock wave.

$$u(x,t) = \begin{cases} 1 & x < \dfrac{1+t}{2} \\ 0 & x > \dfrac{1+t}{2} \end{cases} \tag{3.3}$$

We can discretize this equation as follows:

$$u_i^{n+1} = u_i^n - \frac{\Delta t}{2\Delta x}\left((u_i^n)^2 - (u_{i-1}^n)^2\right) \tag{3.4}$$

Here superscripts refer to time and subscripts to space. This scheme can be referred to as conservative differencing. Consider the following equation:

$$u_t + uu_x - \epsilon u_{xx} = 0 \tag{3.5}$$

We can discretize this equation as follows:

$$u_i^{n+1} = u_i^n - \frac{\Delta t u_i^n}{2\Delta x}\left(u_{i+1}^n - u_{i-1}^n\right) + \frac{\Delta t \epsilon}{\Delta x^2}\left(u_{i+1}^n - 2u_i^n + u_{i-1}^n\right) \tag{3.6}$$

If we allow $\epsilon = .5\Delta x$ we obtain the viscous solution to burgers equation.

This idea leads to the celebrated method of artificial viscosity [36]. We use this concept to stabilize our equations. This method is also known as inconsistent stabilization as opposed to consistent stabilization. Figure 3.1 shows that the quality of the result remains

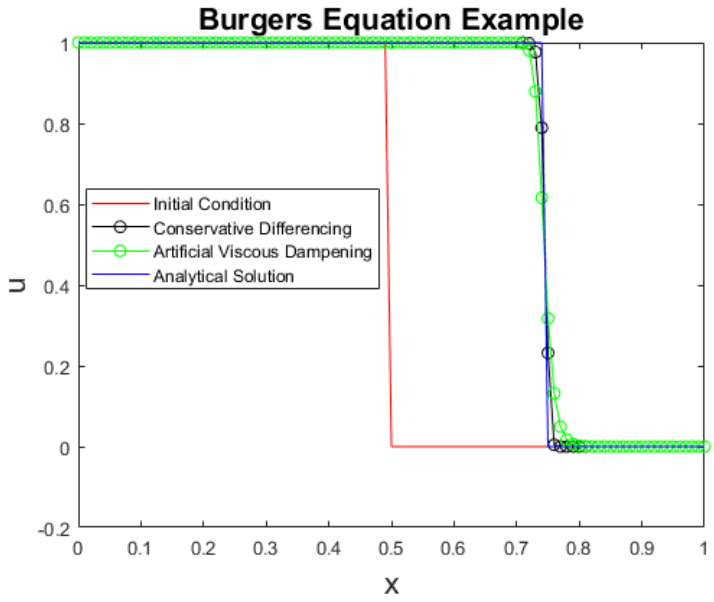

Figure 3.1: All discretizations on top of each other

unchanged by doing so.

3.1.1 Electric Field

In order to have a complete system of equations to solve for evaluating the effectiveness of axisymmetric neoclassical viscosity, we need to have the same number of known equations and unknown variables. In the previous chapter, we had a term called the electric field. We did not explicitly state what the field was equal to. The electric field must be calculated. If we recall the multifluid equations, we can take the electron equation and order out all terms that have a mass dependence. This is because electrons are 1000 times lighter than deuterium. We are left with the following:

$$\nabla p_e + n_e e_e \boldsymbol{E} + n_e e_e \boldsymbol{v}_e \times \boldsymbol{B} + n_e \nu_{de}(\boldsymbol{v_e} - \boldsymbol{v_d}) = 0 \tag{3.7}$$

If we use the fact that a plasma is neutral and that current is the curl of the magnetic field, then the electron momentum balance allows us to write the electric field as in equation

(3.8),

$$\boldsymbol{E} = \frac{\frac{\nabla \times \boldsymbol{B}}{\mu_0} - \sum_j e_j n_j \boldsymbol{V_j}}{\sum_j e_j n_j} \times \boldsymbol{B} - \frac{\nabla(\sum_j Z_j n_j T_e)}{\sum_j e_j n_j} + \eta_r \frac{\nabla \times \boldsymbol{B}}{\mu_0} \tag{3.8}$$

Where η_r is referred to as plasma resistance and takes care of the friction between ions and electrons and is of order $5 \times 10^{-7} \Omega \cdot \text{m}$. This relation is commonly referred to as the generalized *Ohm's law*. The form above is of particular use to numerical simulation and is used in several codes including NIMROD [37]. An important simplification that we will use is that in true steady state, the electric field can also be written as

$$\boldsymbol{E} = \nabla \varphi + \boldsymbol{E^A} \tag{3.9}$$

Where φ is the electric potential and E^A is a small toroidal electric field (.9 V/m) due to induction and resistance. This is important as we will use this to effectively remove any geometric mistakes from the slightly incorrect magnetic field we are using. We additionally set E^A to zero for the simulation we present and also the resistance to zero: this is one area for improvement; however, the difference between the terms we drop and those we keep is three orders of magnitude, so it seems unlikely that any major difference would result from keeping those terms.

3.1.2 Streamline Potential Formulation of Velocity Field

In solving equations (2.60) through (2.63), rather than working directly with vector equations, it is simpler to have scalar equations [38]. To do this, we define the velocity stream function as Ψ, the velocity potential as Φ, and the toroidal velocity as before.

$$\boldsymbol{v} = \nabla \Psi \times \nabla \phi + v_t \boldsymbol{e}_\phi + \nabla \Phi \tag{3.10}$$

$$\boldsymbol{v_t} = v_t \boldsymbol{e}_\phi \tag{3.11}$$

$$\boldsymbol{v_s} = \nabla\Psi \times \nabla\phi \tag{3.12}$$

$$\boldsymbol{v_f} = \nabla\Phi \tag{3.13}$$

Here $\nabla\phi = R^{-1}\boldsymbol{e_\phi}$. If our vector equation can be written as $\boldsymbol{A}(n, \boldsymbol{v}) = 0$ then we can use three different operators in order to obtain three scalar equations. Our equations become

$$-\nabla\phi \cdot \nabla \times \boldsymbol{A} = 0 \tag{3.14}$$

$$R^2\nabla\phi \cdot \boldsymbol{A} = 0 \tag{3.15}$$

$$-\nabla \cdot \boldsymbol{A} = 0 \tag{3.16}$$

In the following sections we describe the specifics of terms in our equations.

Time and Inertial Representation

The time terms become

$$\frac{\partial\nabla^2\Psi}{\partial t} \qquad \frac{\partial\nabla^2\Phi}{\partial t} \qquad \frac{\partial R v_t}{\partial t}$$

The continuity equation has the following inertial term:

$$\nabla \cdot n\boldsymbol{v} = \nabla \cdot n\nabla\Phi - \nabla \cdot \nabla \times (\Psi\nabla\phi). \tag{3.17}$$

The momentum term requires more effort. Our local coordinates are (ρ, θ, ϕ) where ρ is the radial variable, θ is the poloidal variable, and ϕ is the toroidal variable. In local coordinates,

we expand the material derivative:

$$(\boldsymbol{v}\cdot\boldsymbol{\nabla}\boldsymbol{v})_r = \frac{v_p}{h_\theta}\frac{\partial v_r}{\partial\theta} + \frac{v_r}{h_\rho}\frac{\partial v_r}{\partial\rho} - \frac{v_r h_{\rho\theta}}{h_\theta^2 h_\rho}\frac{\partial v_r}{\partial\theta} + \left(\frac{v_p^2}{h_\theta h_\rho}\frac{\partial h_\theta^{-1} h_{\rho\theta}}{\partial\theta} - \frac{v_p^2}{h_\theta h_\rho}\frac{\partial h_\theta}{\partial\rho}\right) + \frac{\partial h_\rho}{\partial\theta}\frac{v_p v_r}{h_\theta h_\rho} + \left(\frac{h_{\rho\theta}v_t^2}{h_\theta^2 h_\rho h_\phi}\frac{\partial h_\phi}{\partial\theta} - \frac{v_t^2}{h_\rho h_\phi}\frac{\partial h_\phi}{\partial\rho}\right), \quad (3.18)$$

$$(\boldsymbol{v}\cdot\boldsymbol{\nabla}\boldsymbol{v})_p = \frac{v_p}{h_\theta}\frac{\partial v_p}{\partial\theta} + \frac{v_r}{h_\rho}\frac{\partial v_p}{\partial\rho} - \frac{v_r h_{\rho\theta}}{h_\theta^2 h_\rho}\frac{\partial v_p}{\partial\theta} + \left(\frac{v_r v_p}{h_\theta h_\rho}\frac{\partial h_\theta}{\partial\rho} - \frac{v_r v_p}{h_\theta h_\rho}\frac{\partial h_\theta^{-1} h_{\rho\theta}}{\partial\theta}\right) - \frac{v_r^2}{h_\theta h_\rho}\frac{\partial h_\rho}{\partial\theta} - \frac{v_t^2}{h_\theta h_\phi}\frac{\partial h_\phi}{\partial\theta}, \quad (3.19)$$

$$(\boldsymbol{v}\cdot\boldsymbol{\nabla}\boldsymbol{v})_t = \frac{v_p}{h_\theta}\frac{\partial v_t}{\partial\theta} + \frac{v_r}{h_\rho}\frac{\partial v_t}{\partial\rho} - \frac{v_r h_{\rho\theta}}{h_\theta^2 h_\rho}\frac{\partial v_t}{\partial\theta} + \frac{v_p v_t}{h_\theta h_\phi}\frac{\partial h_\phi}{\partial\theta} + \frac{v_r v_t}{h_\rho h_\phi}\frac{\partial h_\phi}{\partial\rho} - \frac{h_{\rho\theta}v_r v_t}{h_\theta^2 h_\rho h_\phi}\frac{\partial h_\phi}{\partial\theta}. \quad (3.20)$$

Where we have used the following definitions:

$$h_\rho \equiv |\nabla\rho|^{-1}, \quad (3.21)$$

$$h_\theta \equiv \sqrt{\left(\frac{\partial R}{\partial\theta}\right)^2 + \left(\frac{\partial R}{\partial\theta}\right)^2}, \quad (3.22)$$

$$h_\phi \equiv R, \quad (3.23)$$

$$h_{\rho\theta} \equiv -h_\theta^2 h_\rho^2 \nabla\theta\cdot\nabla\rho. \quad (3.24)$$

Our inertial terms are:

$$-\nabla\phi\cdot\nabla\times(\boldsymbol{v}\cdot\nabla\boldsymbol{v}) = -\nabla\phi\cdot\nabla\times\left((\boldsymbol{v}\cdot\boldsymbol{\nabla}\boldsymbol{v})_r\,\boldsymbol{e_r} + (\boldsymbol{v}\cdot\boldsymbol{\nabla}\boldsymbol{v})_p\,\boldsymbol{e_p} + (\boldsymbol{v}\cdot\boldsymbol{\nabla}\boldsymbol{v})_t\,\boldsymbol{e_t}\right)$$
$$= -\nabla\phi\cdot\nabla\times\left(\boldsymbol{v_t}\cdot\nabla\boldsymbol{v_t} + \boldsymbol{v_s}\cdot\nabla(\boldsymbol{v_s}+\boldsymbol{v_f}) + \boldsymbol{v_f}\cdot\nabla\boldsymbol{v_s}\right), \quad (3.25)$$

$$R^2\nabla\phi\cdot(\boldsymbol{v}\cdot\nabla\boldsymbol{v}) = R^2\nabla\phi\cdot\left((\boldsymbol{v}\cdot\boldsymbol{\nabla v})_r\,\boldsymbol{e_r}+(\boldsymbol{v}\cdot\boldsymbol{\nabla v})_p\,\boldsymbol{e_p}+(\boldsymbol{v}\cdot\boldsymbol{\nabla v})_t\,\boldsymbol{e_t}\right)$$
$$= R^2\nabla\phi\cdot\left(\boldsymbol{v_t}\cdot\nabla\left(\boldsymbol{v_s}+\boldsymbol{v_f}\right)+\left(\boldsymbol{v_s}+\boldsymbol{v_f}\right)\cdot\nabla\boldsymbol{v_t}\right), \tag{3.26}$$

$$-\nabla\cdot(\boldsymbol{v}\cdot\nabla\boldsymbol{v}) = -\nabla\cdot\left((\boldsymbol{v}\cdot\boldsymbol{\nabla v})_r\,\boldsymbol{e_r}+(\boldsymbol{v}\cdot\boldsymbol{\nabla v})_p\,\boldsymbol{e_p}+(\boldsymbol{v}\cdot\boldsymbol{\nabla v})_t\,\boldsymbol{e_t}\right)$$
$$= -\nabla\cdot\left(\boldsymbol{v_t}\cdot\nabla\boldsymbol{v_t}+\left(\boldsymbol{v_s}+\boldsymbol{v_f}\right)\cdot\nabla(\boldsymbol{v_s}+\boldsymbol{v_f})\right). \tag{3.27}$$

Pressure

The pressure terms are

$$\frac{\nabla\phi\cdot\nabla n\times\nabla T}{mn}\approxeq 0 \qquad 0 \qquad \nabla\cdot\frac{\nabla nT}{mn} \tag{3.28}$$

Here the first term is typically called the baroclinic torque and without actually evolving the energy equation, we cannot really say that it is not zero. Additionally, keeping the term mainly affects the iteration process, with minimal effect on the actual solution. The only noticeable effect is that when temperature is assumed to be constant on a flux surface, there is a small shift up of the profiles in the results section.

Electromagnetic

$$term1 = \frac{e}{m}\nabla\cdot\nabla\phi\times\boldsymbol{v}\times\boldsymbol{B} \tag{3.29}$$

$$term2 = \frac{e}{m}RE^A+\frac{e}{m}R(\boldsymbol{v}\times\boldsymbol{B})_\phi \tag{3.30}$$

$$term3 = \frac{e}{m}\nabla\cdot\boldsymbol{E}+\nabla\cdot\frac{e}{m}\boldsymbol{v}\times\boldsymbol{B} \tag{3.31}$$

3.1.3 Viscous Terms

We need to define two terms in order to make writing the equations simpler.

$$\boldsymbol{W}_{\parallel} \equiv \frac{\boldsymbol{\Pi}_{\parallel}}{\eta_0}, \tag{3.32}$$

$$\boldsymbol{W}_{\Omega} \equiv \frac{\boldsymbol{\Pi}_{\Omega}}{\eta_3}. \tag{3.33}$$

Finally, we define the following kinematic viscosity coefficients:

$$\mu^0 \equiv \frac{\eta_0}{mn} \tag{3.34}$$

$$\mu^3 \equiv \frac{\eta_3}{mn} \tag{3.35}$$

Additionally, we have to add in some small artificial viscosities. Again, this is commonly done, and the form of sledgehammer used in this calculation is substantially more refined than the one in NIMROD [39] for instance. Specifically, we need to use three different ones in order to avoid adding in more extra viscosity than needed for numerical purposes.

$$\nabla \cdot \boldsymbol{\Pi} = \nabla \cdot \boldsymbol{\Pi}_{\parallel} + \nabla \cdot \boldsymbol{\Pi}_{\Omega} + \nabla \cdot \varepsilon \boldsymbol{\Pi}_{\Psi} + \nabla \cdot \varepsilon \boldsymbol{\Pi}_{\Phi} + \nabla \cdot \varepsilon \boldsymbol{\Pi}_{t} \tag{3.36}$$

The extra viscous terms are represented as follows:

$$\frac{\nabla \cdot \varepsilon \boldsymbol{\Pi}_{\Psi}}{mn} = \nabla \mu_{\Psi} \nabla^2 \Psi, \tag{3.37}$$

$$\frac{\nabla \cdot \varepsilon \boldsymbol{\Pi}_{\Phi}}{mn} = \nabla \mu_{\Phi} \nabla^2 \Phi, \tag{3.38}$$

$$\frac{\nabla \cdot \varepsilon \boldsymbol{\Pi}_{t}}{mn} = \nabla \mu_{t} \nabla v_t. \tag{3.39}$$

There does exist an optimal amount of viscosity to minimize errors [40], but the technique for doing so is beyond the scope of this work. Recently, this method was implemented for an inviscid plasma [41].

Source terms

The source terms are modeled identically to the other terms.

3.1.4 Actual Equations

The eight equations we arrive at can be written in the following "compact" form:

$$\frac{\partial n_d}{\partial t} + \nabla \cdot n_d \nabla \Phi_d - \nabla \cdot n_d \nabla \times (\Psi_d \nabla \phi) = S_d^0 \tag{3.40}$$

$$\frac{\partial n_c}{\partial t} + \nabla \cdot n_c \nabla \Phi_c - \nabla \cdot n_c \nabla \times (\Psi_c \nabla \phi) = 0 \tag{3.41}$$

$$\begin{aligned} \frac{\partial \nabla^2 \Psi_d}{\partial t} + \nabla \cdot \left(\nabla \phi \times \left(\boldsymbol{v_d} \cdot \nabla \boldsymbol{v_d} + \nabla \cdot \mu^0 \boldsymbol{W}_{\parallel} + \nabla \cdot \mu^3 \boldsymbol{W}_{\Omega} \right) \right) - \nabla^2 \mu_{\Psi} \nabla^2 \Psi_d \\ = \frac{e}{m} \nabla \cdot \nabla \phi \times \boldsymbol{v_d} \times \boldsymbol{B} - \nabla \cdot \frac{S_d^0 \nabla \phi \times \boldsymbol{v_d}}{m_d n_d} + \nabla \cdot \nu_{dc} \nabla \phi \times (\boldsymbol{v_c} - \boldsymbol{v_d}) \end{aligned} \tag{3.42}$$

$$\begin{aligned} \frac{\partial \nabla^2 \Psi_c}{\partial t} + \nabla \cdot \left(\nabla \phi \times \left(\boldsymbol{v_c} \cdot \nabla \boldsymbol{v_c} + \nabla \cdot \mu^0 \boldsymbol{W}_{\parallel} + \nabla \cdot \mu^3 \boldsymbol{W}_{\Omega} \right) \right) - \nabla^2 \mu_{\Psi} \nabla^2 \Psi_c = \\ \frac{e}{m} \nabla \cdot \nabla \phi \times \boldsymbol{v_c} \times \boldsymbol{B} + \nabla \cdot \nu_{cd} \nabla \phi \times (\boldsymbol{v_d} - \boldsymbol{v_c}) \end{aligned} \tag{3.43}$$

$$\begin{aligned} \frac{\partial \nabla^2 \Phi_d}{\partial t} + \nabla \cdot \left(\boldsymbol{v_d} \cdot \nabla \boldsymbol{v_d} + \frac{\nabla p_d}{m_d n_d} + \nabla \cdot \mu^0 \boldsymbol{W}_{\parallel} + \nabla \cdot \mu^3 \boldsymbol{W}_{\Omega} \right) - \nabla^2 \mu_{\Phi} \nabla^2 \Phi_d \\ = \frac{e}{m} \nabla \cdot \boldsymbol{E} + \nabla \cdot \frac{e}{m} \boldsymbol{v_d} \times \boldsymbol{B} + \nabla \cdot \frac{S_d^0 \boldsymbol{v_d}}{m_d n_d} + + \nabla \cdot \nu_{dc} \left(\boldsymbol{v_c} - \boldsymbol{v_d} \right) \end{aligned} \tag{3.44}$$

$$\frac{\partial \nabla^2 \Phi_c}{\partial t} + \nabla \cdot \left(\boldsymbol{v_c} \cdot \nabla \boldsymbol{v_c} + \frac{\nabla p_c}{m_c n_c} + \nabla \cdot \mu^0 \boldsymbol{W}_{\parallel} + \nabla \cdot \mu^3 \boldsymbol{W}_{\Omega} \right) - \nabla^2 \mu_{\Phi} \nabla^2 \Phi_c$$
$$= \frac{e}{m} \nabla \cdot \boldsymbol{E} + \nabla \cdot \frac{e}{m} \boldsymbol{v_c} \times \boldsymbol{B} + \nabla \cdot \nu_{cd} \left(\boldsymbol{v_d} - \boldsymbol{v_c} \right) \quad (3.45)$$

$$\frac{\partial R v_{td}}{\partial t} + R^2 \nabla \phi \cdot \left(\boldsymbol{v_d} \cdot \nabla \boldsymbol{v_d} + \nabla \cdot \mu^0 \boldsymbol{W}_{\parallel} + \nabla \cdot \mu^3 \boldsymbol{W}_{\Omega} \right) - R \nabla \mu_t \nabla v_{td}$$
$$= \frac{e}{m} (R E^A + R^2 \nabla \phi \cdot (\boldsymbol{v_d} \times \boldsymbol{B})) + \frac{R S_d^1 - R S_d^0 v_t}{m_d n_d} + R \nu_{dc} \nabla \phi \times (v_{tc} - v_{td}) \quad (3.46)$$

$$\frac{\partial R v_{tc}}{\partial t} + R^2 \nabla \phi \cdot \left(\boldsymbol{v_c} \cdot \nabla \boldsymbol{v_c} + \nabla \cdot \mu^0 \boldsymbol{W}_{\parallel} + \nabla \cdot \mu^3 \boldsymbol{W}_{\Omega} \right) - R \nabla \mu_t \nabla v_{tc}$$
$$= \frac{e}{m} (R E^A + R^2 \nabla \phi \cdot (\boldsymbol{v_c} \times \boldsymbol{B})) + R \nu_{cd} \nabla \left(v_{td} - v_{tc} \right) \quad (3.47)$$

Solving this system to the steady state solution should allow us to see the rotation velocity (at least as well as the assumption of zero baroclinic effects would allow). Additionally, there is an optimum amount of viscosity to use for the scheme [40]. However, the scheme that is optimum is beyond the scope of this thesis.

3.2 Method Used

After much deliberation and testing of various techniques, we decided to use the spectral Galerkin method to solve our equations. The spectral Galerkin method is equivalent in its formulation to the finite element method, thus the two terms will be used interchangeably. Despite the hyperbolic nature of the equations used in the field, it is not unheard of in the field to use finite elements [42, 43, 31]. The first reason we chose this method is that the finite element method works well with the Fourier expansion in the poloidal direction. The finite volume method cannot handle the use of Fourier expansion in the poloidal direc-

tion. This leaves, by elimination, the finite element method as the best method for both theoretical continuity and physical ordering. Specifically, the reason why a Fourier expansion is attractive is that poloidal asymmetries are thought to be small; therefore, a Fourier expansion in poloidal angle would rapidly approach the true two-dimensional value. Additionally, all other numerical methods can be written as special cases of finite element method. For instance, the finite volume method is identical to the low order discontinuous Galerkin method [44].

3.2.1 Overview of Galerkin Methods

The simplest Galerkin method is the finite element method. To begin the discussion of finite elements, it is useful to provide a simple review. As a toy problem, consider the diffusion equation.

$$u_t + \nabla \cdot D\nabla u = S \tag{3.48}$$

If we multiply this equation by a test function v, then we can integrate it over a volume.

$$\int u' v dV + \int v\nabla \cdot D\nabla u dV = \int v S dV \tag{3.49}$$

The integration by parts formula gives us

$$\int u' v d^3x - \int \nabla v \cdot D\nabla u dV + \oint v D\nabla u dS = \int v S d^3x \tag{3.50}$$

If we assume that we have a system of test basis function which equal 0 on the boundary, we can write this as

$$\int u' v_i d^3x - \int \nabla v_i \cdot D\nabla u dV = \int v_i S dV \tag{3.51}$$

Assume that

$$u \cong \sum a_i(t) v_i \tag{3.52}$$

Additionally label

$$M_{ij} = \int v_i v_j dV \tag{3.53}$$

$$K_{ij} = \int \nabla v_i \cdot \nabla v_j dV \tag{3.54}$$

$$S_i = \int v_i S dV \tag{3.55}$$

Then we have

$$\boldsymbol{M}\boldsymbol{a}' + D\boldsymbol{K}\boldsymbol{a} = \boldsymbol{S} \tag{3.56}$$

Which is easy to solve. This is the essence of finite elements.

3.2.2 Galerkin Weak Formulation of Rotation Problem

Here we develop our variational form for the rotation problems. We begin by developing a number of functionals, which we will call *forms* so that we can write the equation for our system in an abbreviated formula. Our weak formulation is as follows. Define our mass operators as follows:

$$MC[u, v] \equiv \int u\, v \, \mathrm{d}V \tag{3.57}$$

$$MS[u, v] \equiv \int \nabla u \cdot \nabla v \, \mathrm{d}V \tag{3.58}$$

$$MT[u, v] \equiv \int R\, u\, v \, \mathrm{d}V \tag{3.59}$$

$$MP[u, v] \equiv \int \nabla u \cdot \nabla v \, \mathrm{d}V \tag{3.60}$$

We have the following forms:

$$VC[u, v, \boldsymbol{w}] \equiv \int \nabla u \cdot v\boldsymbol{w} \, \mathrm{d}V \tag{3.61}$$

$$VS[u, \boldsymbol{w}; \boldsymbol{v}] \equiv \int \nabla u \cdot (\nabla\phi \times \boldsymbol{w} \cdot \nabla \boldsymbol{v}) \, \mathrm{d}V \tag{3.62}$$

$$VT[u, \boldsymbol{w}; \boldsymbol{v}] \equiv \int R\, u\, \boldsymbol{w} \cdot \nabla \boldsymbol{v} \cdot \boldsymbol{e}_{\boldsymbol{\phi}} \, \mathrm{d}V \tag{3.63}$$

$$VP[u, \boldsymbol{w}; \boldsymbol{v}] \equiv \int \nabla u \cdot (\boldsymbol{v} \cdot \nabla \boldsymbol{w}) \, \mathrm{d}V \tag{3.64}$$

$$PP[u, v; w] \equiv \int \nabla \frac{u}{w} \cdot \nabla v T \, \mathrm{d}V \tag{3.65}$$

The viscous weak forms:

$$B_D C[u, v] \equiv -\int D\nabla u \cdot \nabla v \, \mathrm{d}V \tag{3.66}$$

$$B_{\parallel} S[u, \boldsymbol{w}] \equiv \int \nabla(\nabla u \otimes \big(\nabla\phi)\times : \mu^0 \boldsymbol{W}_{\parallel}[\boldsymbol{w}]\big) \, \mathrm{d}V \tag{3.67}$$

$$B_{\parallel} T[u, \boldsymbol{w}] \equiv -\int \nabla(R\, u) \cdot \mu^0 \boldsymbol{W}_{\parallel}[\boldsymbol{w}] \cdot \boldsymbol{e}_{\boldsymbol{\phi}} \, \mathrm{d}V \tag{3.68}$$

$$B_{\parallel} P[u, \boldsymbol{w}] \equiv \int \nabla\nabla u : \mu^0 \boldsymbol{W}_{\parallel}[\boldsymbol{w}] \, \mathrm{d}V \tag{3.69}$$

Here equation (3.67) is somewhat odd, but makes sense in component form.

$$B_{\Omega} S[u, \boldsymbol{w}] \equiv \int \nabla(\nabla u \otimes \big(\nabla\phi)\times : \mu^3 \boldsymbol{W}_{\Omega}[\boldsymbol{w}]\big) \, \mathrm{d}V \tag{3.70}$$

$$B_{\Omega} T[u, \boldsymbol{w}] \equiv -\int \nabla(R\, u) \cdot \mu^3 \boldsymbol{W}_{\Omega}[\boldsymbol{w}] \cdot \boldsymbol{e}_{\boldsymbol{\phi}} \, \mathrm{d}V \tag{3.71}$$

$$B_{\Omega} P[u, \boldsymbol{w}] \equiv \int \nabla\nabla u : \mu^3 \boldsymbol{W}_{\Omega}[\boldsymbol{w}] \, \mathrm{d}V \tag{3.72}$$

And the artificial forms:

$$B_a S[u, \boldsymbol{w}] \equiv \int \nabla(\nabla u \otimes (\nabla \phi) \times : \boldsymbol{W}_{\Psi}[\boldsymbol{w}]) \ \mathrm{d}V \tag{3.73}$$

$$B_a T[u, \boldsymbol{w}] \equiv - \int \nabla(R\, u) \cdot \boldsymbol{W}_{\phi}[\boldsymbol{w}] \cdot \boldsymbol{e_{\phi}} \ \mathrm{d}V \tag{3.74}$$

$$B_a P[u, \boldsymbol{w}] \equiv \int \nabla \nabla u : \boldsymbol{W}_{\Phi}[\boldsymbol{w}] \ \mathrm{d}V \tag{3.75}$$

The Electromagnetic "source" terms are as follows:

$$ET[u] \equiv \int R\, u \frac{e}{m} E^A \ \mathrm{d}V \tag{3.76}$$

$$\begin{aligned} EP[u] \equiv & -\frac{e}{m} \int \nabla u \cdot \frac{\frac{\nabla \times \boldsymbol{B}}{\mu_0} - \sum_j e_j n_j \boldsymbol{v_j}}{\sum_j e_j n_j} \times \boldsymbol{B} \ \mathrm{d}V \\ & + \frac{e}{m} \int \nabla u \cdot \frac{\nabla(\sum_j Z_j n_j T_e)}{\sum_j e_j n_j} - \nabla u \cdot \frac{e\, \eta_r \nabla \times \boldsymbol{B}}{m\, \mu_0} \ \mathrm{d}V \end{aligned} \tag{3.77}$$

The normal electromagnetic terms are given as:

$$E_b S[u, \boldsymbol{w}] \equiv - \int \frac{e}{m} \nabla u \cdot (\nabla \phi \times \boldsymbol{w} \times \boldsymbol{B}) \ \mathrm{d}V \tag{3.78}$$

$$E_b T[u, \boldsymbol{w}] \equiv \int \frac{e}{m} R\, u\, \boldsymbol{w} \times \boldsymbol{B} \cdot \boldsymbol{e_{\phi}} \ \mathrm{d}V \tag{3.79}$$

$$E_b P[u, \boldsymbol{w}] \equiv - \int \frac{e}{m} \nabla u \cdot (\boldsymbol{w} \times \boldsymbol{B}) \ \mathrm{d}V \tag{3.80}$$

The source terms are given as:

$$SC[u] \equiv \int u S^0 \mathrm{d}V \tag{3.81}$$

$$ST[u] \equiv \int u \nabla \phi \cdot \frac{\boldsymbol{S^1}}{m\, n} \mathrm{d}V \tag{3.82}$$

$$B_S S[u, \boldsymbol{w}] \equiv \int \nabla u \cdot \frac{S^0 \nabla \phi \times \boldsymbol{w}}{m\, n} \mathrm{d}V \tag{3.83}$$

$$B_S T[u, \boldsymbol{w}] \equiv -\int u \nabla \phi \cdot \frac{S^0 \boldsymbol{w}}{m\, n} \mathrm{d}V \tag{3.84}$$

$$B_S P[u, \boldsymbol{w}] \equiv \int \nabla u \cdot \frac{S^0 \boldsymbol{w_d}}{m\, n} \mathrm{d}V \tag{3.85}$$

Finally we have the friction terms, which are identical to the other terms and left out for the sake of brevity.

3.2.3 Combined Residual Formulation

The following combined terms can be defined:

$$BC[u, v] = B_D C[u, v] \tag{3.86}$$

$$BS[u, \boldsymbol{w}] = B_\parallel S[u, \boldsymbol{w}] + B_\Omega S[u, \boldsymbol{w}] + B_a S[u, \boldsymbol{w}] - E_b S[u, \boldsymbol{w}] - B_S S[u, \boldsymbol{w}] \tag{3.87}$$

$$BT[u, \boldsymbol{w}] = B_\parallel T[u, \boldsymbol{w}] + B_\Omega T[u, \boldsymbol{w}] + B_a T[u, \boldsymbol{w}] - E_b T[u, \boldsymbol{w}] - B_S T[u, \boldsymbol{w}] \tag{3.88}$$

$$BP[u, \boldsymbol{w}] = B_\parallel P[u, \boldsymbol{w}] + B_\Omega P[u, \boldsymbol{w}] + B_a P[u, \boldsymbol{w}] - E_b P[u, \boldsymbol{w}] - B_S P[u, \boldsymbol{w}] \tag{3.89}$$

We additionally define the residuals:

$$\boldsymbol{RCD}[u] = BC_d[u, n_d] + SC_d[u] + VC_d[u, n_d; \boldsymbol{v_d}] \tag{3.90}$$

$$\boldsymbol{RCC}[u] = BC_c[u, n_c] + VC_d[u, n_c; \boldsymbol{v_c}] \tag{3.91}$$

$$\boldsymbol{RSD}[u] = BS_d[u, \boldsymbol{v_d}] + SS_d[u] + VS_d[u, \boldsymbol{v_d}; \boldsymbol{v_d}] \tag{3.92}$$

$$\boldsymbol{RSC}[u] = BS_c[u, \boldsymbol{v_d}] + SS_c[u] + VS_c[u, \boldsymbol{v_c}; \boldsymbol{v_c}] \tag{3.93}$$

$$\boldsymbol{RTD}[u] = BT_d[u, \boldsymbol{v_d}] + ST_d[u] + VT_d[u, \boldsymbol{v_d}; \boldsymbol{v_d}] \tag{3.94}$$

$$\boldsymbol{RTC}[u] = BT_c[u, \boldsymbol{v_d}] + ST_c[u] + VT_c[u, \boldsymbol{v_c}; \boldsymbol{v_c}] \tag{3.95}$$

$$\boldsymbol{RPC}[u] = BP_d[u, \boldsymbol{v_d}] + PP_c[u, n_d; n_d] + SP_d[u] + VP_d[u, \boldsymbol{v_d}; \boldsymbol{v_d}] \tag{3.96}$$

$$\boldsymbol{RPD}[u] = BP_c[u, \boldsymbol{v_d}] + PP_c[u, n_c; n_c] + SP_c[u] + VP_c[u, \boldsymbol{v_c}; \boldsymbol{v_c}] \tag{3.97}$$

Where u is a test function. The point we want to make here is that our system is solved when our residuals are zero. Let $u,\ n_d,\ n_c\ , \Phi_d,\ \Phi_c,\ \Psi_d,\ \Psi_c,\ v_{td},\ v_{tc}$ be from the same finite element space; then, define the vector residual:

$$\boldsymbol{R}_i = \begin{pmatrix} \boldsymbol{RCD}[u_i] \\ \boldsymbol{RCC}[u_i] \\ \boldsymbol{RSD}[u_i] \\ \boldsymbol{RSC}[u_i] \\ \boldsymbol{RTD}[u_i] \\ \boldsymbol{RTC}[u_i] \\ \boldsymbol{RPC}[u_i] \\ \boldsymbol{RPD}[u_i] \end{pmatrix} \tag{3.98}$$

Define the solution vector $\boldsymbol{\Omega}$ the same way.

3.3 Remark on the creation of the code

The equations above were developed using Mathematica [45]. These mathematical equations ensured that no mistakes were made in using the Miller [18] coordinate system. The resulting equations are hundreds of thousands of lines long, proving the utility of the mathematical software. These equations are converted into Fortran 2008 code. They are then compiled using the Intel Fortran compiler ifort19 with the highest optimization settings. OpenMP and SIMD are used to vectorize and parallelize some key loops in the assembly of the finite element matrix. The NAG library is used to create the quadrature for the integrals [30]. The grid used is a 51 point Chebyshev Gauss-Lobatto grid [30]. Our weights are computed using a Clenshaw-Curtis quadrature accurate up to a fiftieth order polynomial [30]. Some numerical experimentation has shown that this is sufficiently accurate for triple products of up to twenty fifth order Bessel functions, with a five hundredth order quadrature only being $\sim .1\%$ more accurate. The calculation of the residual and occasionally an

approximate Jacobian is performed in bulk then assembled with the specific test and base functions. This leads to an extremely efficient method for solving these equations.

3.4 Approximation and Test Space

The method presented above is considered to be conforming. This is because of the elements belonging to the same approximation space. The conforming method works best in a Bessel-Fourier-Galerkin approach. This sort or approach is sometimes called a spectral element approach, and a similar spectral Galerkin approach was very recently [39] used to solve the ideal plasma equilibrium, also known as the Grad–Shafranov equation. Therefore, this likely represent the first spectral Galerkin solution to the non-ideal plasma equilibrium.

The use of Fourier elements has a natural radial analog, Bessel functions. The advantage of Bessel function expansions is that they ensure a smooth solution to the FEM problem. The disadvantage is that a Bessel solution can only handle Dirichlet boundary conditions. This is only a disadvantage insofar as it requires more input data than a Neumann boundary condition. Unfortunately, this biases the solutions calculated to be more correct at the edge than they would otherwise be; however, piecewise elements can still be used, and initial testing with such elements shows that they produce similar results when subjected to the same boundary conditions. The use of other boundaries results in some oscillations that would require a more sophisticated method to avoid.

In this approach, the functions are expanded as follows:

$$n = n_0 + \sum\sum a_{ij} J_i\left(\lambda_{ij}\rho\right)\cos\left(j\theta\right) + b_{ij} J_i\left(\lambda_{ij}\rho\right)\sin\left(j\theta\right) \tag{3.99}$$

$$\psi = \psi_0 + \sum\sum a_{ij} J_i\left(\lambda_{ij}\rho\right)\cos\left(j\theta\right) + b_{ij} J_i\left(\lambda_{ij}\rho\right)\sin\left(j\theta\right) \tag{3.100}$$

$$\phi = \phi_0 + \sum\sum a_{ij} J_i\left(\lambda_{ij}\rho\right)\cos\left(j\theta\right) + b_{ij} J_i\left(\lambda_{ij}\rho\right)\sin\left(j\theta\right) \tag{3.101}$$

$$v_t = v_{t0} + \sum\sum a_{ij} J_i\left(\lambda_{ij}\rho\right)\cos\left(j\theta\right) + b_{ij} J_i\left(\lambda_{ij}\rho\right)\sin\left(j\theta\right) \tag{3.102}$$

Where the subscript 0 is a function chosen to satisfy boundary conditions The lambda represents the 0 of the Bessel function being used. Due to a restriction known as the CFL restriction, an implicit method is required in order to solve this in a timely manner [46]. We have the following backward Euler method:

$$\boldsymbol{M}\Delta t(\boldsymbol{\Omega}^{n+1} - \boldsymbol{\Omega}^{n}) = -\boldsymbol{R}^{n+1} \tag{3.103}$$

This is done for a few seconds (which is by far long enough). We then use a method known as the Jacobian-Free-Newton-Krylov to resolve the residuals to near zero [47]. Overall this leads to a relatively quick method to solve these equations that converges rapidly with respect to the order of the expansion. For instance, a second order radial expansion with a fourth order poloidal expansion is almost as good as a twelfth order radial expansion with tenth order poloidal expansion.

CHAPTER 4

RESULTS

Using the methods presented in the previous chapter, we solved the equations presented at the end of chapter 2 in order to address our goal set forth in chapter 1; specifically, we desire to predict as accurately as possible the two-dimensional toroidal rotation profile prescribed by axisymmetric neoclassical theory in order to determine the accuracy of axisymmetric neoclassical theory.

We performed a twelfth order radial and a tenth order poloidal expansion resulting in 2016 degrees of freedom in our system to obtain our results. This is not a practical level of refinement for performing "routine" analysis of experiments, but a lower order may prove to be a very practical alternative. Our initial guesses were fixed at the boundary values in order to ensure that we were not predisposed to obtain the solutions of the experiment. We used the finite element streamline–potential formulation of the velocity equations from the previous chapter in order to advance the equations implicitly to steady state and performed Newton's method of iteration to remove any lingering residuals.

On all of our plots, we show calculated values at four poloidal locations for each normalized ρ value, along with a spline fit of the experimental data. The empty square points are from automated spline fits based upon experimental data or processed data: some of the fits actually have no data to back them up. The worst offender is the deuterium poloidal velocity, whose "experimental" value is based upon no poloidal variation of any terms and an electric field derived from the carbon radial momentum balance.

$$v_{\theta d} = \frac{1}{n_d e_d B_\phi} \left(-\nabla p_d - n_d e_d E_r + n_d e_d v_\phi B_\theta \right) \tag{4.1}$$

This level of approximation produces what appears to be a very wrong data set for the

deuterium poloidal velocity.

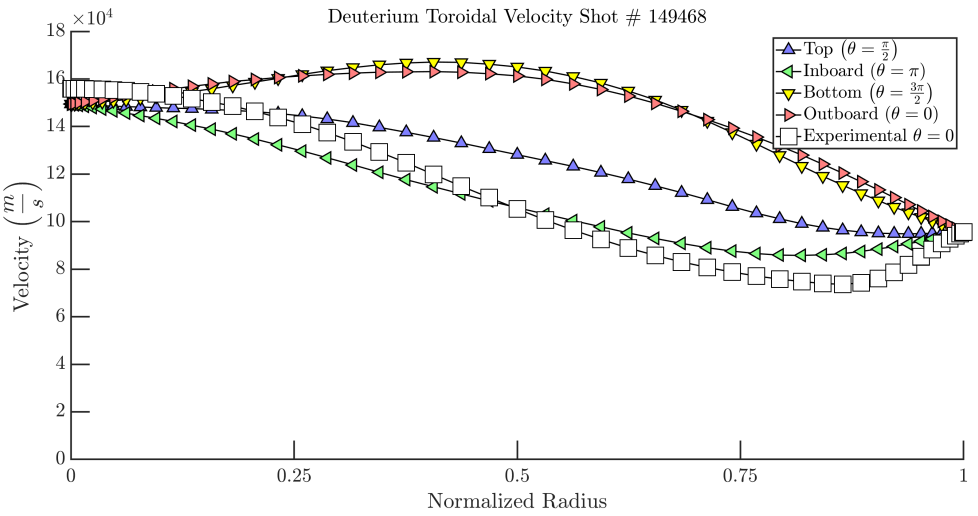

Figure 4.1: DIII-D Shot # 149468. Deuterium toroidal velocity vs measured data.

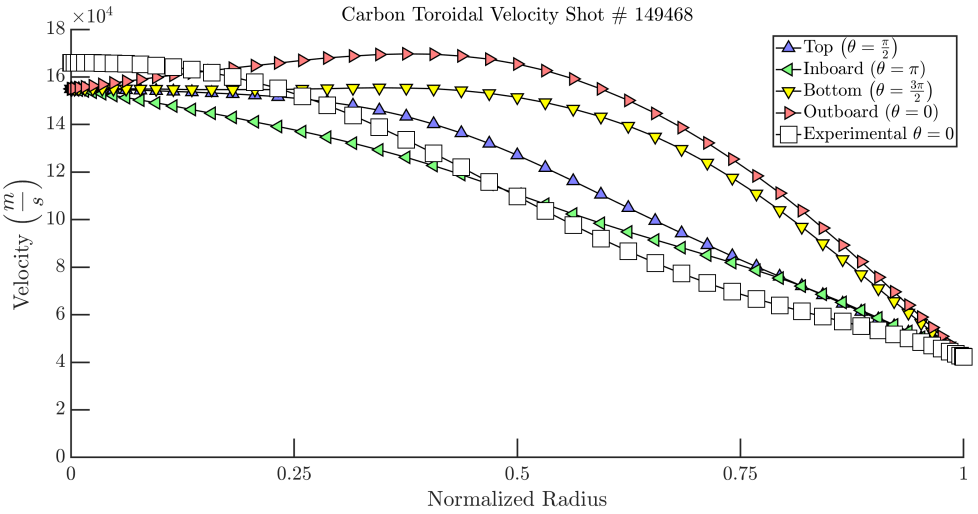

Figure 4.2: Carbon toroidal velocity vs measured data.

Figure 4.1 and 4.2 show that we over-predict the toroidal velocity by a slight amount especially at the edge. This is likely due to non-axisymmetric effects [48] causing a large viscous term to appear in the edge that is not included in any theory.

Figure 4.3 and 4.4 show that we under predict the deuterium density when compared to measured or inferred data. This is somewhat expected for reasons elaborated latter.

Figure 4.5 and 4.6 show that we predict the carbon poloidal rotation to within about

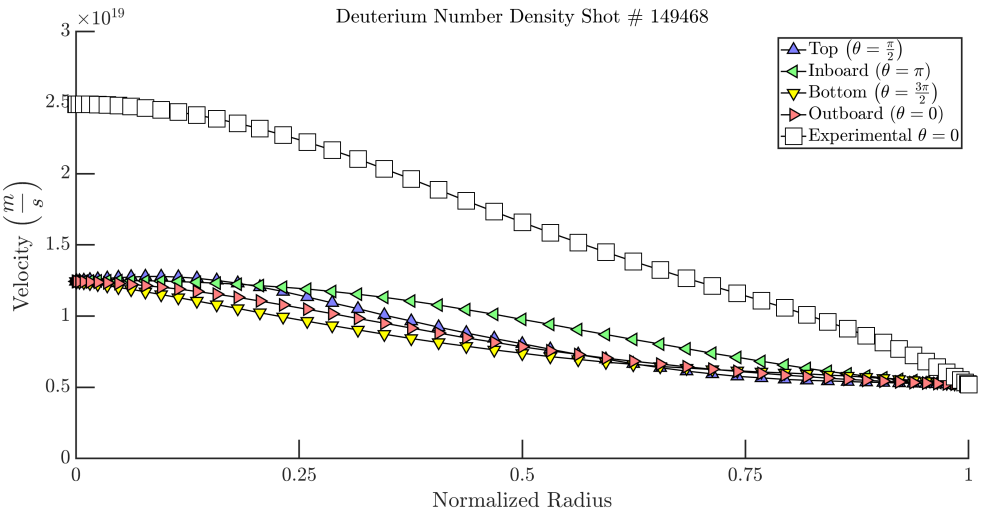

Figure 4.3: Deuterium inferred density vs calculated

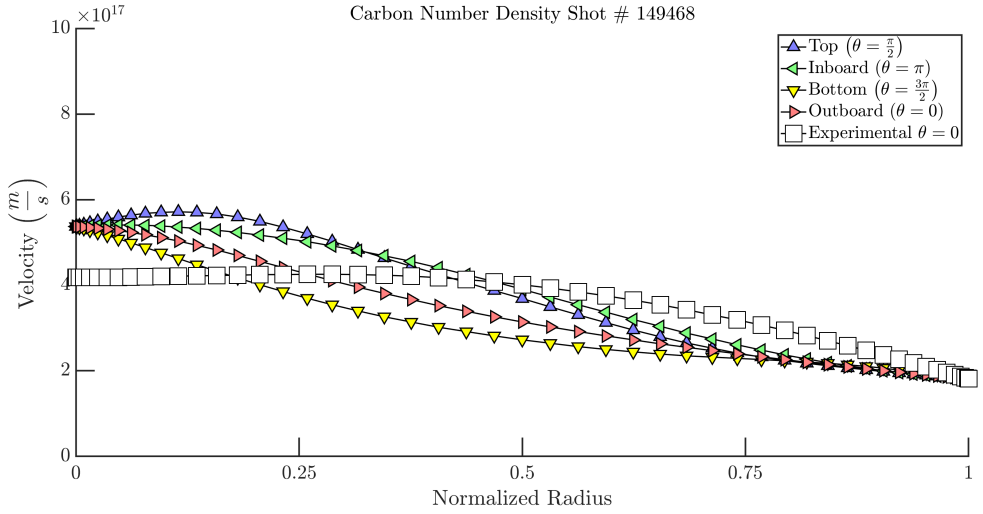

Figure 4.4: Carbon inferred density vs calculated

10% and that either the inferred deuterium poloidal rotation velocity is wrong or that the calculation of deuterium's velocity is wrong.

Figure 4.7 and 4.8 show that poloidal asymmetries of radial fluxes are very high compared to the typical assumption of no radial flux asymmetry. his assumption is brought on by the fact that the average radial flow should be either zero or some small number related to the deposition of particles.

The deuterium has significant poloidal asymmetries in radial flows. This exacerbates

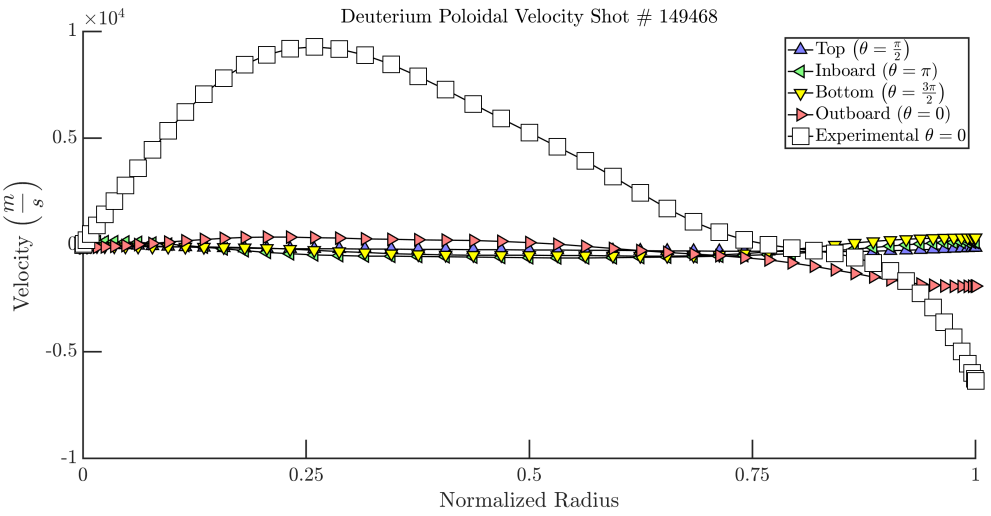

Figure 4.5: The deuterium poloidal velocity vs inferred poloidal rotation.

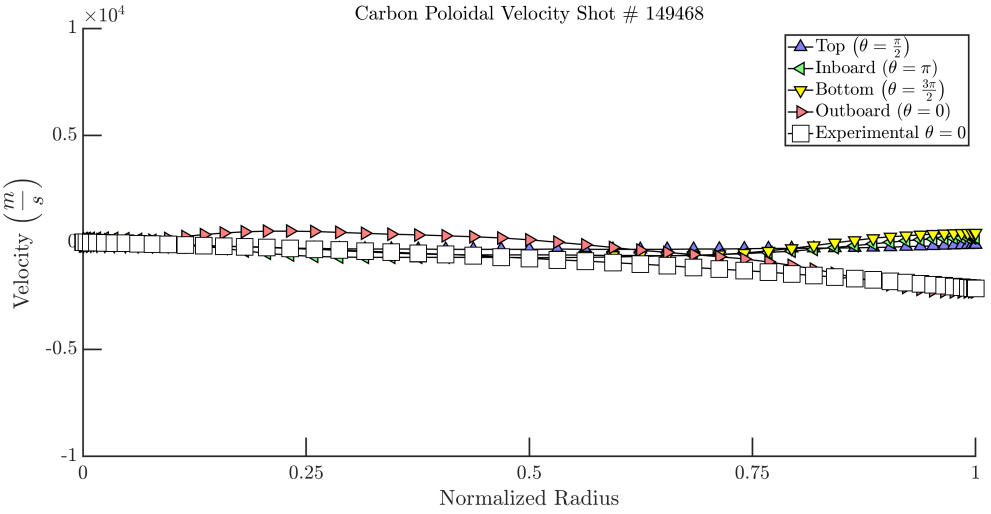

Figure 4.6: The carbon poloidal velocity vs measured poloidal rotation.

the fact that there is a net outflow by obfuscating the measurement of such a flow. The fact is that the asymmetries are of higher magnitude than the bulk. The carbon radial velocity is significant but on average zero. The asymmetries present here show that non-flux surface aligned flows are important. A later diagram shows the interesting effect of this asymmetry.

An important concept in visualization of fluid calculations is the flow visualization. The flow refers to how a massless test particle would move if it was dropped in the fluid. Since

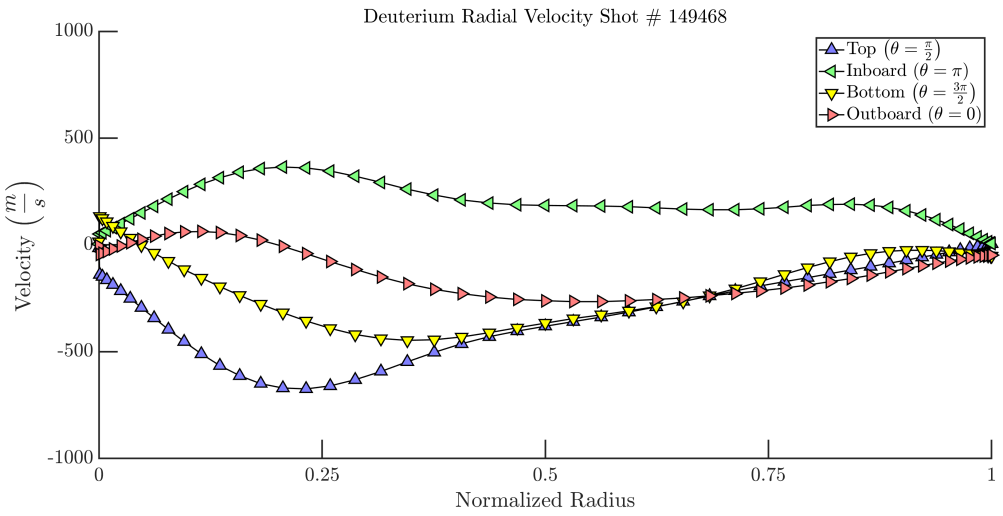

Figure 4.7: Deuterium calculated radial velocity.

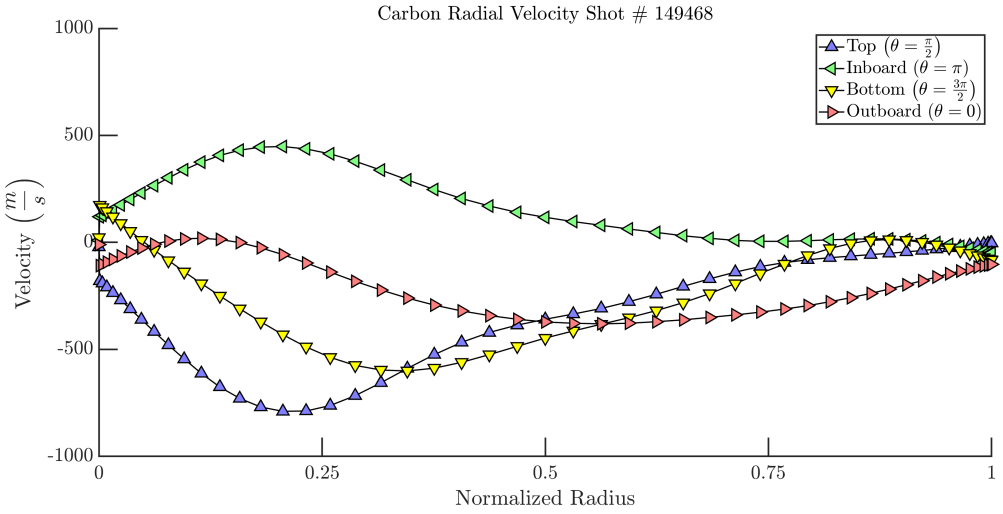

Figure 4.8: Carbon calculated radial velocity.

the particle is massless, it would move at the velocity of the fluid.

$$\frac{d\boldsymbol{x}}{dt} = \boldsymbol{v}(\boldsymbol{x}) \tag{4.2}$$

If we expand this into component form, we obtain:

$$\frac{d\rho}{dt} = \frac{v_r(\rho,\theta)}{h_\rho} \tag{4.3}$$

$$\frac{d\theta}{dt} = \frac{v_p(\rho,\theta)}{h_\theta} - \frac{h_{\rho\theta}v_r(\rho,\theta)}{h_\theta^2 h_\rho} \tag{4.4}$$

$$\frac{d\phi}{dt} = \frac{v_t(\rho,\theta)}{h_\phi} \tag{4.5}$$

If we plot the trajectories of (ρ,θ) for several starting positions, we get the flow of the fluid. Each of these trajectories is called a streamline. Much information is available from the streamlines, such as the divergence and the convection.

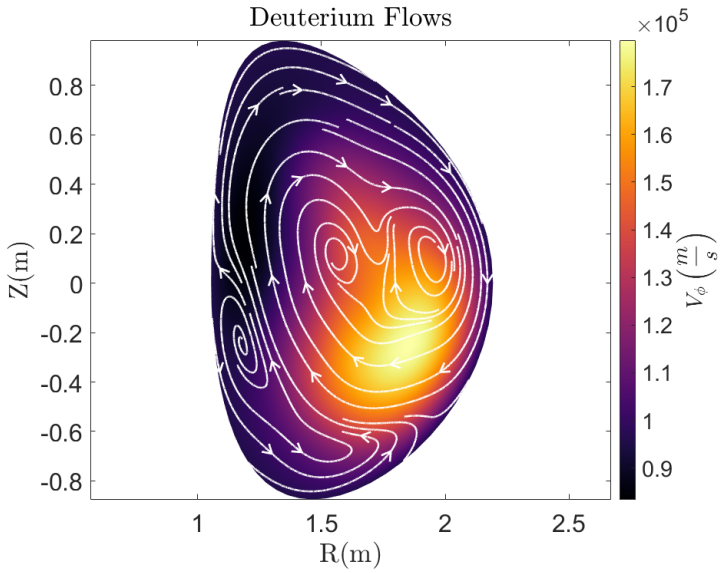

Figure 4.9: The lines show the flow of the deuterium. The color represents the toroidal velocity of the deuterium.

Figure 4.9 and 4.10 show the poloidal asymmetries of the toroidal velocities plotted on top of the flow. The flow shows an interesting outward directed shift of the typically assumed vortex flow for a tokamak. Specifically, what is observed is that the asymmetries appear to create a non-flux surface aligned flow. This mismatch appears to be driven by centrifugal effects due to the outward directedness of it. This result may have a number of

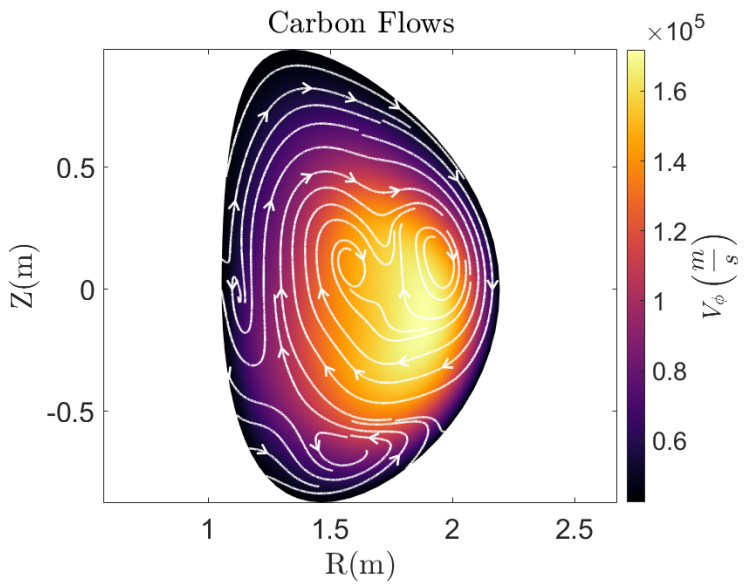

Figure 4.10: The lines show the flow of the carbon. The color represents the toroidal velocity of the carbon.

consequences.

4.1 Boundary Values

One issue with this method is the requirement of a boundary condition. While we have a wide variety of boundary values to choose from, we must still choose one without any real justification. A skeptic might state that we determine the magnitude of the rotation (which is more important than the profile) by setting the boundary condition. The skeptic might want to then know the sensitivity of the solutions magnitude to the magnitude of the solution. This can be evaluated by setting the boundary value to zero and observing if we are of the same order of magnitude. As we can see from figures 4.11 and 4.12, the order of magnitude is unaffected by the boundary condition. Therefore, the skeptic should be quite happy.

Additionally, we might attempt to make a first principles estimate of the toroidal veloc-

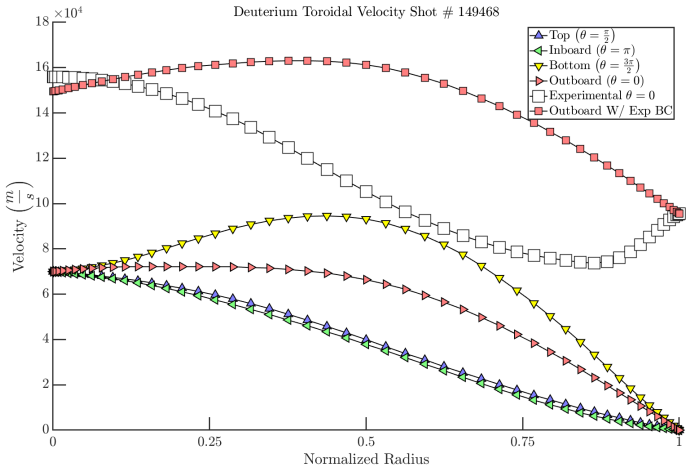

Figure 4.11: Deuterium solution with zero BC. The calculation was done in low order to save time.

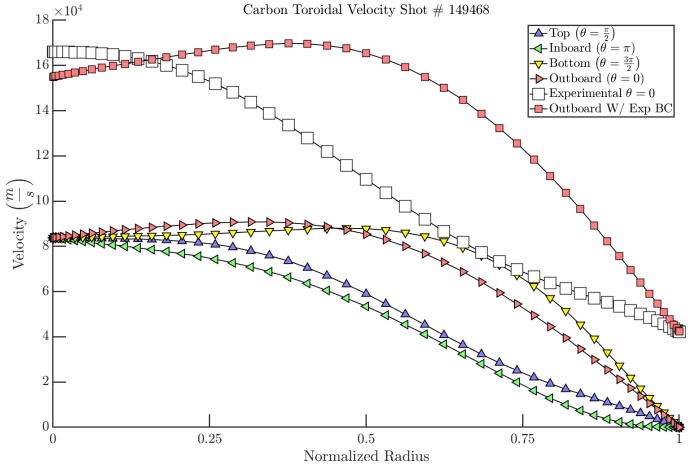

Figure 4.12: Carbon solution with zero BC. The calculation was done in low order to save time.

ity at the edge. If we assume there is a boundary layer, we can calculate that

$$|v_\phi| \approxeq \frac{2qL_\phi}{L_\theta}|v_\theta| \tag{4.6}$$

The poloidal velocity does not need to be specified on the boundary and thus we have a first principle iteration scheme, we set the toroidal velocity along the boundary to be a multiple of the poloidal velocity. This would converge in one iteration for this shot. Figure 4.13 is

an example of this procedure.

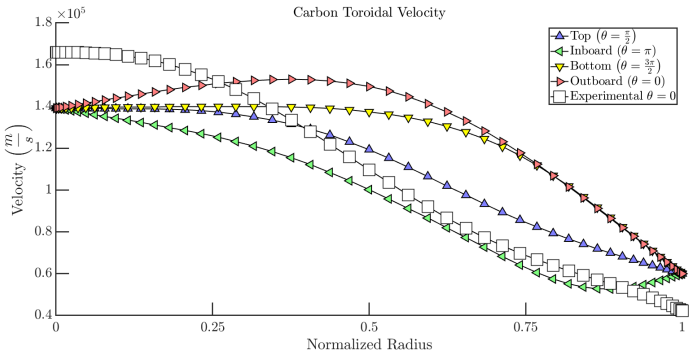

Figure 4.13: Carbon solution with theoretically inspired boundary condition. The calculation was done in low order to save time.

4.2 Discussion

Our results represent an improvement when compared to previous results of roughly 15%. The fact of the matter is that most codes are either 1D such as PROCTR, or 3D such as NIMROD or only focus on the plasma edge such as UEDGE and SOLPS. This makes it rather difficult to actually even compare the results here to others since most codes to do this sort of thing never leave the lab they are created in.

We can see that the predicted value of toroidal velocity for both carbon and deuterium without the use of an anomalous transport; we are very close on poloidal velocities, and are densities are low. The last point is to be expected since we use a non-conservative scheme and we have an artificial diffusion. Even fully non-dissipative schemes with no artificial viscosity or diffusion such as the semi-Lagrangian tend to have an issue with leaking that has to be alleviated through some means or ignored [49]. This means that even where the model fails, it is to be expected and other models of the same variety would fail.

An important point is that the inferred poloidal deuterium rotation is either incorrect or the calculation of such a number is incorrect. This is only possible if we assume no poloidal asymmetries. Under that assumption, the radial velocity of carbon must be identically zero; the radial velocity of deuterium is just a simple integral; the toroidal velocity of carbon is

measured, and the toroidal velocity of deuterium can be either measured or inferred relatively easily. If we have the deuterium toroidal velocity already, we can then use the radial momentum balance of the deuterium to calculate the poloidal velocity via equation (4.1). The argument against is that it has been observed that the magnitude calculated by these methods seems to be in complete disagreement with measured data every time measurements have been available [50]. The toroidal velocity we predict is also significantly better than what is seen in reference [50].

A comparison can be found by looking into a recent study [51] that accounted for asymmetries to a degree. They found a reasonable agreement of poloidal flows with measured data after accounting for the asymmetries of the flow. The unfortunate matter is still that analysis which accounts for asymmetries in the radial flow do not compare with experiment. Another unfortunate matter is that it is unlikely to ever have measurements of radial velocity asymmetries due to the relatively small speed and the limited space for diagnostic systems.

This all boils down into the simple statement that our hypothesis appears to be true. Axisymmetric neoclassical viscosity seems to do a reasonable job in predicting the toroidal and poloidal flows. With the level of accuracy, it would seem suspicious to claim that anomalous or turbulent effects would govern the flow. It is, however, open for examination, that this might be a fluke. That most other experiments would be impossible to explain with this theory. On the other hand, it seems reasonable to claim that neoclassical theory should not be thrown out without further investigation into whether 2d effects can allow accurate prediction for other experiments.

CHAPTER 5
CONCLUSION

In this thesis, we have sought to evaluate how well toroidally axisymmetric neoclassical gyroviscosity performs at predicting toroidal rotation. We can conclude that neoclassical viscosity performs remarkably well at matching experimental data, at least to within a factor of two. We have created a fully 2-dimensional streamline potential conforming spectral Galerkin model that is globally conservative and produces reasonable answers. Where the model fails, it is to be expected and other models of the same variety would fail too. Possible extensions to this model include accounting for non-axisymmetric effects, accounting for error fields, using a locally conservative form, and performing more validation.

This model represents an extension of work previously done at Georgia ech [1, 2, 3, 4, 5, 6, 7, 8, 9] and this thesis, to a degree, represents a culmination of that formalism. The extensions include high degrees of poloidal representation including a tenth order Fourier expansion, removal of the separation of variables assumption, and removal of the gradient scale length formalism. Future work is still needed. Experiments conducted with resonant magnetic perturbation feature non-axisymmetric effects and non-axisymmetric effects are important [52]. Furthermore, this level of refinement is not practical routine analysis of experiments. This is a major downside, but a lower order may prove to be a very practical alternative.

Additionally, this work is different from other state-of-the-art models in several effects. The first is the use of neoclassical gyroviscosity. The second is the separation of the magnetic field evolution from the rotation problem. The third is the lack of an anomalous transport mechanism. These three main differences are well complemented by computational differences. The main computational difference is the use of a spectral Galerkin method to represent the profiles. This representation ensures that stability will remain so long as

spectral pollution remains small [53].

The dominant conclusion of this thesis is that when performed to the degree of accuracy required, axisymmetric neoclassical gyroviscosity can represent toroidal rotation damping very well when the poloidal asymmetries are properly represented, and that these effects, which are often ordered away, must be accurately accounted for in order to have any hope of predicting the toroidal rotation of a plasma. This is of vital importance for new larger tokamaks such as ITER since these devices should ideally have few instabilities happening. The shear flows that have been calculated here should also give some good news for ITER. The primary effect of the asymmetries is to balance out the centrifugal forces due to the rotation. This means that having a much larger major radius should increase the toroidal rotation by decreasing the gyroviscous damping. This is simply a hypothesis that should be tested in future work.

Appendices

APPENDIX A

BASIC PARTIAL DIFFERENTIAL EQUATION THEORY

This mainly defines some notation and terms used throughout the thesis.

A.1 Multi-Index

Let $\Omega \subset \mathbb{R}^n$. Let $x \in \Omega$. Let $u : \Omega \to \mathbb{R}$. Let $\alpha \in \mathbb{N}^n$. Define the modulo $|\alpha| := \alpha_1 + \alpha_2 + \cdots + \alpha_n = \sum \alpha_i$. We introduce the notion of $D^{\alpha_i}_{x_i} u := \frac{\partial^{\alpha_i} u}{\partial x_i^{\alpha_i}}$. We extend this is the multi-index derivative defined as

$$D^{\alpha} u := \frac{\partial^{\alpha_1}}{\partial x_1^{\alpha_1}} \frac{\partial^{\alpha_2}}{\partial x_2^{\alpha_2}} \cdots \frac{\partial^{\alpha_n}}{\partial x_n^{\alpha_n}} u(x). \tag{A.1}$$

A.2 What is a PDE

From Evans [54], "A *partial differential equation* (PDE) is an equation involving an unknown function of two or more variables and certain of its partial derivatives." This is a rather broad definition; however, we do not deal with simple PDEs exclusively, but also with systems of PDEs. Going on, a PDE is implicitly defined as being:

$$F(D^k u, D^{k-1} u, \cdots, u, x) = 0 \tag{A.2}$$

where x is a multi-index variable [54].

The four main types of PDEs are *linear*, *semilinear*, *quasilinear*, and *fully nonlinear* [54]. Linear PDEs can be written in the form:

$$\sum_{|\alpha| \leq k} a_{\alpha}(x) D^{\alpha} u = f(x) \tag{A.3}$$

A homogenous linear PDE is a PDE where f is 0 [54].

A semilinear PDE is a PDE where:

$$\sum_{|\alpha|=k} a_\alpha(x) D^\alpha u + a_0(D^{k-1}u, \cdots, u, x) = 0 \tag{A.4}$$

A quasilinear PDE:

$$\sum_{|\alpha|=k} a_\alpha(D^{k-1}u, \cdots, u, x) D^\alpha u + a_0(D^{k-1}u, \cdots, u, x) = 0 \tag{A.5}$$

And a fully nonlinear PDE is everything else. It is worth noting that for semilinear PDEs, it should be obvious that if $\forall \alpha : \ |\alpha| = k, |a_\alpha(x)| \equiv 0$, then this is not really a semilinear PDE. In fact, if this happens on any subset of the domain with a positive measure, then for all intents and purposes, then the PDE is fully nonlinear.

A.2.1 Examples

The simplest linear PDE is the one speed wave equation:

$$\begin{cases} u_t(t,x) + u_x(t,x) = 0 & \text{in } (0,\infty) \times \mathbb{R}, \\ u(0,\cdot) = u_0 & \text{on } \{t=0\} \times \mathbb{R}. \end{cases} \tag{A.6}$$

This has the solution:

$$u(t,x) = u_0(x-t). \tag{A.7}$$

A simple semilinear equation is:

$$\nabla^2 u(x) = -\frac{|x|^2 u(x)}{4} \qquad \text{in } \Omega \subset \mathbb{R}^3.$$

Here if we let omega be a spherical shell with constant on the inside and outside for the boundaries, the solution is:

$$u = \frac{c_1}{\sqrt{\|x\|}} + \frac{c_2 \log \|x\|}{\sqrt{\|x\|}}. \tag{A.8}$$

The simplest quasilinear PDE is burgers equation:

$$\begin{cases} u_t + uu_x = 0 & (x,t) \in \mathbb{R} \times (0,\infty), \\ u = g & (x,t) \in \mathbb{R} \times \{0\}. \end{cases} \tag{A.9}$$

Define [54]:

$$y(x,t) \equiv \arg\min_{y \in \mathbb{R}} \left(\frac{(x-y)^2}{2t} + \int_0^y g(z)\mathrm{d}z \right) \tag{A.10}$$

This has a closed form solution given by Lax and Oleinik [54]:

$$u(x,t) = \frac{x - y(x,t)}{t} \tag{A.11}$$

The simplest nonlinear PDE is the Eikonal equation.

$$|\nabla u| = 1 \tag{A.12}$$

This gives the nearest distance from the boundary as its solution.

A.3 Important Terms

The Laplace operator is

$$\Delta u \equiv \nabla^2 u = \text{div}\,(\text{grad}\ u) \tag{A.13}$$

where ∇ is the usual.

Any function that satisfies the so-called Laplace's equation

$$-\Delta u = 0 \tag{A.14}$$

is referred to as a *harmonic* function [54]. Harmonic functions have many important properties. The first important property is that if a function is harmonic then, for any ball of radius ϵ around a point x_0

$$u(x_0) = \frac{\int\limits_{\|x-x_0\|<\epsilon} u(x)dx}{\alpha(n)\epsilon^n} = \frac{\int\limits_{\|x-x_0\|=\epsilon} u(x)dS}{n\alpha(n)\epsilon^{n-1}} \tag{A.15}$$

Where alpha is the volume of the n dimensional hyper-sphere [54].

Another important property of harmonic functions is that they satisfy the maximum principle. That is to say, on any sub-domain of a harmonic function, both the maximum and the minimum value are attained on the boundary. Furthermore, if the maximum is obtained anywhere on the interior, then the function must be constant everywhere, this includes on all other connected subdomains.

A.4 Conservation Equations

A system of k equations that can be written as

$$\begin{aligned} U_t^1 + \text{div}\left(F^1(U^1, U^2, \cdots, U^k)\right) &= 0 \\ U_t^2 + \text{div}\left(F^2(U^1, U^2, \cdots, U^k)\right) &= 0 \\ &\vdots \\ U_t^k + \text{div}\left(F^k(U^1, U^2, \cdots, U^k)\right) &= 0 \end{aligned}$$

Where, F is called a flux, is referred to as a system of k conservation equations [54].

A.5 Weak Form

A weak form of a PDE is an integral form of the PDE. The intregral form requires fewer derivatives than the differential form, and the solution to the weak form of the PDE only satisifies the PDE almost everywhere. The idea of a weak form of a PDE comes from the integration by parts formula. We say that, $u \in L^\infty$ is a weak solution to a PDE $L(u) = 0$ whenever $\int vL(u)\mathrm{d}x = 0$ for all $v \in C_c^\infty$. Take as an example a system of conservation laws.

$$\begin{cases} \boldsymbol{u}_t + \nabla \cdot \boldsymbol{F}(\boldsymbol{u}) = 0 & (\boldsymbol{x}, t) \in \Omega \times (0, \infty) \\ \boldsymbol{u}(\boldsymbol{x}, 0) = \boldsymbol{g}(x) & \{t = 0\} \times \boldsymbol{x} \in \Omega \end{cases} \tag{A.16}$$

We have for our weak form:

$$\int_0^\infty \int_\Omega \boldsymbol{v}_t \cdot \boldsymbol{u}\mathrm{d}\boldsymbol{x}\mathrm{d}t + \int_0^\infty \int_\Omega \boldsymbol{F}\left(\boldsymbol{u}\right) : \nabla \boldsymbol{v}\mathrm{d}\boldsymbol{x}\mathrm{d}t + \int_\Omega \boldsymbol{g}(x)\boldsymbol{v}(\boldsymbol{x}, 0)\mathrm{d}\boldsymbol{x} = 0. \tag{A.17}$$

This concept is at the heart of every Galerkin method. Let $\mathcal{L}[\boldsymbol{u}] \equiv \boldsymbol{c}\boldsymbol{u} + \nabla \cdot \boldsymbol{M}\nabla \boldsymbol{u}$. The system in this thesis is of the form:

$$\begin{cases} \mathcal{L}[\boldsymbol{u}]_t + \boldsymbol{b}\nabla \boldsymbol{F}(\boldsymbol{u}) + \nabla \cdot \boldsymbol{A}\nabla \boldsymbol{u} + \nabla^2 \boldsymbol{K}\nabla^2 \boldsymbol{u} = \boldsymbol{S} & (\boldsymbol{x}, t) \in \Omega \times (0, \infty) \\ \boldsymbol{u}(\boldsymbol{x}, 0) = \boldsymbol{g}(x) & \{t = 0\} \times \boldsymbol{x} \in \Omega \\ \boldsymbol{f}_1(\boldsymbol{u}, \nabla \boldsymbol{u}, \nabla^2 \boldsymbol{u}) = \boldsymbol{h}_1(\boldsymbol{x}) & (\boldsymbol{x}, t) \in \partial\Omega \times (0, \infty) \\ \boldsymbol{f}_2(\boldsymbol{u}, \nabla \boldsymbol{u}, \nabla^2 \boldsymbol{u}) = \boldsymbol{h}_2(\boldsymbol{x}) & (\boldsymbol{x}, t) \in \partial\Omega \times (0, \infty) \end{cases} \tag{A.18}$$

The weak form of this sort of system is:

$$\int_0^\infty \int_\Omega \left(-\boldsymbol{c}^T \boldsymbol{v}_t + \boldsymbol{M}\nabla \boldsymbol{v}_t\right) \cdot \boldsymbol{u} \, \mathrm{d}\boldsymbol{x} \, \mathrm{d}t - \int_\Omega \boldsymbol{v} \, \boldsymbol{c} \, \boldsymbol{g} \, \mathrm{d}\boldsymbol{x}\Big|_{t=0} - \int_0^\infty \oint_{\partial\Omega} \boldsymbol{v} \cdot \boldsymbol{M}\nabla \boldsymbol{u} \cdot \hat{\boldsymbol{n}} \, \mathrm{d}S \, \mathrm{d}t$$
$$- \oint_{\partial\Omega} \boldsymbol{v} \cdot \boldsymbol{M}\nabla \boldsymbol{u} \cdot \hat{\boldsymbol{n}} \, \mathrm{d}S\Big|_{t=0} + \int_0^\infty \int_\Omega \boldsymbol{v} \cdot \boldsymbol{b}\nabla \boldsymbol{F}(\boldsymbol{u}) \, \mathrm{d}\boldsymbol{x} \, \mathrm{d}t - \int_0^\infty \int_\Omega \nabla \boldsymbol{v} \cdot \boldsymbol{A} \cdot \nabla(\boldsymbol{u}) \, \mathrm{d}\boldsymbol{x} \, \mathrm{d}t$$
$$- \int_0^\infty \oint_{\partial\Omega} \boldsymbol{v} \cdot \boldsymbol{A} \cdot \nabla(\boldsymbol{u}) \cdot \hat{\boldsymbol{n}} \, \mathrm{d}S \, \mathrm{d}t + \int_0^\infty \int_\Omega \nabla^2 \boldsymbol{v} \cdot \boldsymbol{K} \cdot \nabla^2(\boldsymbol{u}) \, \mathrm{d}\boldsymbol{x} \, \mathrm{d}t - \int_0^\infty \oint_{\partial\Omega} \boldsymbol{v} \cdot \nabla \boldsymbol{K} \cdot \nabla^2(\boldsymbol{u}) \cdot \hat{\boldsymbol{n}} \, \mathrm{d}S \, \mathrm{d}t$$
$$+ \int_0^\infty \oint_{\partial\Omega} \nabla \boldsymbol{v} \cdot \boldsymbol{K} \cdot \nabla^2(\boldsymbol{u}) \cdot \hat{\boldsymbol{n}} \, \mathrm{d}S \, \mathrm{d}t = \int_0^\infty \int_\Omega \boldsymbol{S} \cdot \boldsymbol{v} \, \mathrm{d}\boldsymbol{x} \, \mathrm{d}t \quad \text{(A.19)}$$

A.6 Parabolic, Elliptic, and Hyperbolic

The three main types equations are parabolic, elliptic, and hyperbolic. To begin, we will focus on only 2D cases. Consider:

$$A\frac{\partial^2 u}{\partial t^2} + B\frac{\partial^2 u}{\partial t \partial x} + C\frac{\partial^2 u}{\partial x^2} + D\frac{\partial u}{\partial t} + E\frac{\partial u}{\partial x} + Fu = G \quad \text{(A.20)}$$

Let $\Delta = B^2 - 4AC$. If $\Delta = 0$ then we have a parabolic equation such as the heat equation. If $\Delta > 0$ then we have a hyperbolic equation such as the wave equation, system of conservation equations, or the transport equation. If $\Delta < 0$ then we have an elliptic equation such as the Poisson equation. These have analogues in higher dimensional spaces, and higher order PDEs often are analogous to one of these types of PDEs as well.

APPENDIX B

FLUX SURFACE GEOMETRY

It is often convenient to define flux coordinates. The typical flux system coordinate system is given by (ψ, χ, ϕ). We first revisit the MHD momentum equations [10]

$$\nabla p = \boldsymbol{j} \times \boldsymbol{B}. \tag{B.1}$$

We also have from Maxwell's equations

$$\mu_0 \boldsymbol{j} = \nabla \times \boldsymbol{B} \tag{B.2}$$

and

$$\nabla \bullet \boldsymbol{B} = 0. \tag{B.3}$$

We define a flux surface an isobaric surface, with flux value given by ψ.

$$\psi \equiv \frac{\int_{S_p} \boldsymbol{B}_p \bullet \mathrm{d}\boldsymbol{s}_p}{2\pi} = \frac{\int_{S_p} \boldsymbol{B} \bullet \mathrm{d}\boldsymbol{s}_p}{2\pi}. \tag{B.4}$$

To prove that this is independent of orientation in axisymmetry,

$$\frac{d}{dt}\boldsymbol{u} = \frac{\hat{\phi} \times \nabla p}{|\nabla p|} = \frac{\hat{\phi} \times \boldsymbol{j} \times \boldsymbol{B}}{|\nabla p|}. \tag{B.5}$$

We know that the trace of $\boldsymbol{u}$ is on an isobaric surface locally by

$$\nabla p \bullet \frac{d}{dt}\boldsymbol{u} = \nabla p \bullet \hat{\phi} \times \nabla p = 0. \tag{B.6}$$

We also know it exist by the local existence theorem. Make ψ depend on orientation.

$$\psi(t) = \frac{\int_{S_p(t)} \boldsymbol{B} \bullet \mathrm{d}\boldsymbol{s(t)}_p}{2\pi} = \frac{\int_0^s \boldsymbol{B}(\boldsymbol{r}(s)) \bullet \frac{d}{dt}\boldsymbol{u}\mathrm{d}s}{2\pi}. \tag{B.7}$$

$$\nabla\psi(t) = \frac{\int_0^s \nabla(\boldsymbol{B}(\boldsymbol{r}(s)) \bullet \frac{d}{dt}\boldsymbol{u})\mathrm{d}s}{2\pi} = \frac{\int_0^s \boldsymbol{B}(\boldsymbol{r}(s))\nabla \bullet \boldsymbol{u}_t + \frac{\boldsymbol{u}_t \times \boldsymbol{J}}{\mu_0} + \boldsymbol{B} \times \nabla \times \boldsymbol{u}_t \mathrm{d}s}{2\pi}. \tag{B.8}$$

$$\nabla\psi(t) = \int_0^s \frac{\boldsymbol{u}_t \times \boldsymbol{J}}{2\pi\mu_0}\mathrm{d}s \tag{B.9}$$

Which gives us.

$$\nabla\psi(t) \bullet \frac{d}{dt}\boldsymbol{u} = \int_0^s \frac{\boldsymbol{u}_t \times \boldsymbol{J} \bullet \frac{d}{dt}\boldsymbol{u}}{2\pi\mu_0}\mathrm{d}s = 0. \tag{B.10}$$

Therefore, ψ is constant on a flux surface. Flux surfaces are given by the Grad Shafranov equation [10].

B.1 First Order Perfect Equilibrium

This section is adapted from Grad and Rubin. It is included for completeness.

The first order equilibrium of a plasma is given by: [55]

$$\nabla p = \boldsymbol{J} \times \boldsymbol{B}$$

$$\nabla \times \boldsymbol{B} = \mu_0 \boldsymbol{J}$$

$$\nabla \cdot \boldsymbol{B} = 0$$

Let S be a surface. Define $\nabla_S \phi$ to be the projection of the gradient of phi onto the tangent space of S. A vector field is a *surface gradient* with respect to S if the line integral

around any closed surface in S is 0 [55]. If $\boldsymbol{n} \perp S$ then, $\boldsymbol{Y} = \boldsymbol{n} \times \boldsymbol{X}$ is the *conjugate* vector field [55]. A vector field is considered to be a harmonic with respect to S if it is both a surface gradient and a surface curl.

In equilibrium, the pressure gradient is perpendicular to current. Combined with Faraday's law, we obtain that B is a surface gradient [55]. This causes it to be possible to write [55]

$$\boldsymbol{B} = \frac{1}{R}\boldsymbol{e_\phi} \times \nabla\psi + B_\phi \boldsymbol{e_\phi} \tag{B.11}$$

$$\Delta^*\psi + \mu_0 R^2 p'(\psi) + \mu_0 f'(\psi) = 0 \tag{B.12}$$

$$\Delta^* = \frac{\partial^2}{\partial R^2} - \frac{1}{R}\frac{\partial}{\partial R} + \frac{\partial^2}{\partial Z^2} \tag{B.13}$$

Again, these equations are taken directly from [55] and adapted to conform notationally with the rest of the thesis.

B.2 Flux Surface Average

The flux surface average (FSA) is an operator which is defined as being the average value on a flux surface. This is not the same as the average surface integral.

$$\langle F \rangle \equiv \frac{\int F(\psi, \theta, \phi)\sqrt{g}\,\mathrm{d}\phi\,\mathrm{d}\theta}{\int \sqrt{g}\,\mathrm{d}\phi\,\mathrm{d}\theta} \tag{B.14}$$

APPENDIX C

NON-ORTHOGONAL COORDINATES

Non-orthogonal coordinates, also known as skew coordinates, appear often in the analysis of plasmas. In particular, the coorinate system used in this thesis is an example of a skew coordinate system. In order to bridge the difference between a physical and a mathematical understanding of the coordinate system, it becomes necessary to be extreamely precise in the meaning of our coordinates.

To begin, we define what a skew coordinate system is. Skew coordinate systems are coordinate systems in which the isobars of the coordinates (the grid) intersect at angles that are not always 90 degrees. Examples of skew coordinates include elliptical toroidal coordinates, miller flux surface coordinates, and basic skew coordinates.

The following notation shall be used:

- ∇ without a dot represents the gradient.
- $\nabla\cdot$ represents the divergence.
- abc represents that abc is a scalar.
- $\boldsymbol{abc}$ represents that abc is a vector.
- $\mathbf{abc}$ represents that abc is a second rank tensor.
- ABC represents that abc is a space.
- ABC^* represents the duel space of ABC.
- TM will represent vector fields in $\mathbb{R}^3$.

C.0.1 Definitions

As a note, we work in a finite-dimensional **Hilbert space**. A Hilbert space is a vector space equipped with an **inner product**. This means that we have a dot product. A **differentiable manifold** M is a set that can be parameterized by smooth functions of several variables [56]. As an example Let $M = \{(x, y, z) : x^2 + y^2 + z^2 = 1\}$, is a sphere, and can be parameterized as $x(u, v) = \cos(u)\cos(v)$, $y(u, v) = \sin(u)\cos(v)$, and $z(u, v) = \sin(v)$. More precisely, a differentiable manifold includes all such parameterizations. Further, denote the set of all smooth multivariate functions on M as $\mathfrak{D}(M)$ [56]. For our purposes M is $\mathbb{R}^3$ with a coordinate system x attached.

A **vector** can be thought of as generalization of a **tangent vector**. Let $\alpha(t) : \mathbb{R} \to M$ be a curve on a differentiable manifold M and $f \in \mathfrak{D}(p)$, then the tangent vector at $p = \alpha(0)$ is $\alpha'(0) : \mathfrak{D}(M) \to \mathbb{R}$ is a functional that satisfies the following

$$\alpha'(0)f = \left.\frac{df(\alpha(t))}{dt}\right|_{t=0}. \tag{C.1}$$

We then have that a vector can be thought of as a direction derivative operator [56].

$$\alpha'(0) = \sum x_i'(0)\frac{\partial}{\partial x_i} \tag{C.2}$$

This leads us to **covectors**. Covectors are linear functionals that when applied to vectors yield real numbers. For example let y be a covector on a manifold with parameterized with cartesian coordinates at the point $(x, y, z) = (1, 0, 0)$ defined as $y(V(f)) = \int dy V(f)$ and $\alpha(t) = (1, t, 0)$ then

$$y(\alpha'(0)f) = f \tag{C.3}$$

This immediately reveals a more useful definition, a covector maps a vector to a field. Additionally, a covector can be expressed in terms of differentials; whereas, vectors can be written as a sum of partials. Intuitively, we have that $dx^i \perp \partial_j \ \ \forall \ \ j \neq i$.

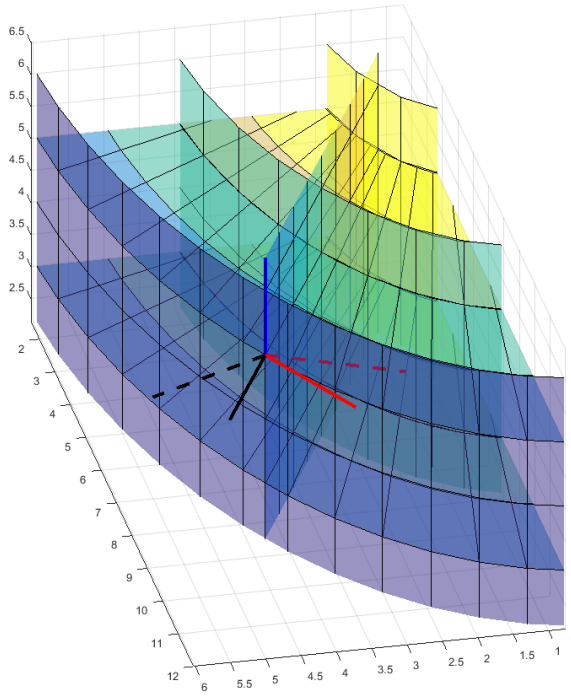

Figure C.1: Here we have a diagram of the covariant and contravariant coordinate bases. The coordinate system is $(r\cos(\theta), 2r\sin(\theta), z)$. The tangent bundle is spaned by the solid lines and the cotangent bundle by the dotted lines. Black is the r component, red is the theta component, blue is the z component. For visualization purposes, all of the vectors were normalized.

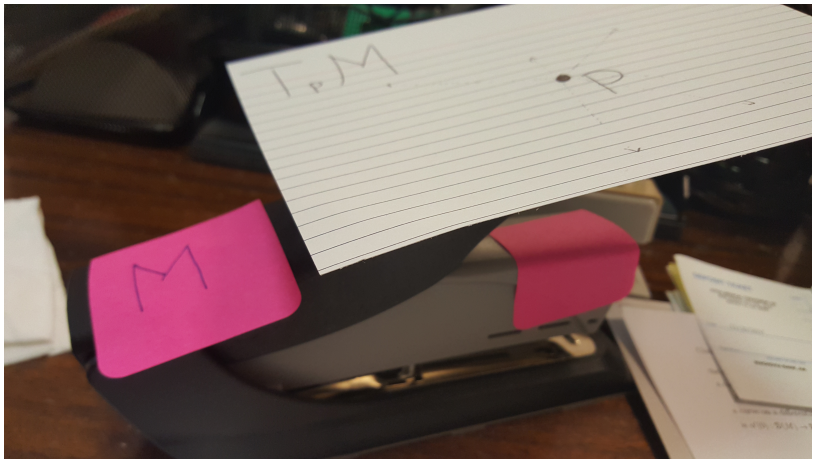

Figure C.2: Here M is the surface of this stapler and the index card represents the tangent plane at the point p where the card is taped to the stappler.

A **vector field** can be thought of as a vector at every point which lays flat on the surface of M. In other words, a vector field takes the set of smooth functions and returns the set of possible directional derivatives [56]. Identify the space of permissible directions at a point p on M as the **tangent plane** at p represented by T_pM and the union of all tangent plane, identified with their points as the **tangent bundle** represented by TM [56]. Physically the tangent plane at a point in the span of configurations a rigid rod can take when placed on a surface at a point. This means that a vector field is a mapping $X : M \to TM$; whereas, a vector is a mapping $V : TM \to \mathbb{R}$ [56]. Intuitively, a vector field then is a mapping from the set of differentiable functions on M into the set of functions on M. This does not generalize well. We identify the set of smooth vector fields on M by $\mathfrak{X}(M)$ [56].

There also exist **covector fields**. Since $\mathbb{R}^n$ is a Hilbert space with a norm, $\langle \cdot, \cdot \rangle$, and is finite dimensional, the dual space is TM^* is isomorphic to TM, where we can assign $V^*(X) = \langle V, X \rangle \, \forall X \in TM$. Covectors are the stars, and $\mathfrak{X}^*(M)$ is the set of covector fields, in the cotangent bundle. We now have that vectors fields can be a linear mapping from the cotangent bundle into the underlying field and covector fields are a linear mapping from the tangent bundle into the underlying field.

A **tensor** T of rank r and type (m, n) on M is a multi-linear mapping,

$$T : \underbrace{\mathfrak{X}(M) \cdots \times \mathfrak{X}(M)}_{n} \times \underbrace{\mathfrak{X}^*(M) \cdots \times \mathfrak{X}^*(M)}_{m} \to \mathfrak{D}(M)$$

where n is the number of covariant components and m is the number of contravariant components [56]. Tensors can be written in terms of a local frame, also known as component form [56]. Let $Y_i \in \mathfrak{X}(M)$ and $\chi_i \in \mathfrak{X}^*(M)$, then with the basis$\{\mathbf{E_i}\}$ we write the component form of T as

$$\begin{aligned} &T(Y_1, \cdots, Y_n, \chi_1, \cdots, \chi_m) \\ &\qquad = \sum_{i_1 \cdots i_n, j_1 \cdots j_m} y_{i_1} \ldots y_{i_n} \chi_{j_1} \ldots \chi_{j_m} T(E_{i_1}, \cdots, E_{i_n}, E^*_{j_1}, \cdots, E^*_{j_m}) \\ &\qquad\qquad = \sum y_{i_1} \ldots y_{i_n} \chi_{j_1} \ldots \chi_{j_m} T^{j_1 \ldots j_m}_{i_1 \ldots i_r} \end{aligned} \tag{C.4}$$

This means that T can be written as

$$T = T^{j_1 \ldots j_n}_{i_1 \ldots i_m} dx^{i_1} \cdots dx^{i_m} \frac{\partial}{\partial x^{j_1}} \cdots \frac{\partial}{\partial x^{j_n}} \tag{C.5}$$

The most important second order tensor is the **metric tensor**. Let g be a second order tensor of type (0,2) that yields the inner product on M [56].

$$g_{ij} = \langle \partial_i, \partial_j \rangle \tag{C.6}$$

An **orthonormal basis** $\{\mathbf{e_j}\}$ is a set of unit vector which satisfy $\mathbf{e_i} \bullet \mathbf{e_j} = \delta_{ij}$ where δ_{ij} is the Kronecker delta [29]. This yields two different ways of representing vector fields

$$X(p) := \sum_{i=1}^{n} a_i(p) \frac{\partial}{\partial x_i} \equiv \sum_{i=1}^{n} b_i(p) \mathbf{e_i} \tag{C.7}$$

A moving **coordinate frame** $\{E_i(q)\}$ is a set of vector fields which form a basis at

every $q \in M$. This is less strict than an orthonormal basis. One of the most common frames to use is the local coordinate frame $\{\partial_i\}$.

$$\partial_i = \frac{\partial}{\partial x^i} \tag{C.8}$$

Since, this frame depends on the coordinate system, it may be best to label it ∂_{x_i}. Other frames can be used.

Second rank tensors can often be represented by **dyads**. A dyad is a double vector. In most formulae, dyads are preferred to the wealth of tensor notation; however, dyads require more care when dealing with addition, since there needs to be a correspondence between the vector spaces of the terms being added together. To this effect, the vector space and the dual space need to be distinguished. The unit dyadic is a tensor product of the basis and the dual basis. This yields

$$\mathbf{I} = \sum_i \mathbf{e_i}^* \otimes \mathbf{e_i} \tag{C.9}$$

APPENDIX D

COORDINATE SYSTEM

We use Miller toroidal flux surface geometry [18], with a few modifications [6] as our coordinate system. For the local vector frame to express vectors in, and orthogonalize the basis [9]. Doing this yields (slightly) different equations than the canonical ones.

The vector basis is given as:

$$\begin{aligned} E_1 &= \frac{1}{h_\rho} D_\rho - \frac{h_{\rho\theta}}{h_\theta^2 h_\rho} D_\theta \\ E_2 &= \frac{1}{h_\theta} D_\theta \\ E_3 &= \frac{1}{h_\phi} D_\phi \end{aligned}$$

Whereas our dual basis is:

$$\begin{aligned} e_1 &= h_\rho d\rho, \\ e_2 &= \frac{h_{\rho\theta}}{h_\theta} d\rho + h_\theta d\theta, \\ e_3 &= h_\phi d\phi. \end{aligned}$$

To obtain the connection coefficients, we shall use the following definition of the Levi–Civita connection [56]:

$$\begin{aligned} \langle Z, \nabla_Y X \rangle = \frac{1}{2} \left(X \langle Y, Z \rangle + Y \langle Z, X \rangle - Z \langle X, Y \rangle - \langle [X, Z], Y \rangle \right. \\ \left. - \langle [Y, Z], X \rangle - \langle [X, Y], Z \rangle \right), \end{aligned} \quad \text{(D.1)}$$

where

$$[X, Y](f) = X(Y(f)) - Y(X(f)).$$

It is worth pointing out that $[X, Y] = -[Y, X]$. Remember that we have E_3 pointing in the toroidal direction,

$$[E_1, E_1] = 0 \tag{D.2}$$

$$[E_1, E_2] = -\frac{1}{h_\theta} D_\theta \left[\frac{1}{h_\rho}\right] D_\rho + \left(\frac{1}{h_\rho} D_\rho \left[\frac{1}{h_\theta}\right] + \frac{1}{h_\theta} D_\theta \left[\frac{h_{\rho\theta}}{h_\theta^2 h_\rho}\right] - \frac{h_{\rho\theta}}{h_\theta^2 h_\rho} D_\theta \left[\frac{1}{h_\theta}\right]\right) D_\theta \tag{D.3}$$

$$[E_1, E_3] = \frac{1}{h_\rho} D_\rho \left[\frac{1}{h_\phi}\right] D_\phi - \frac{h_{\rho\theta}}{h_\theta^2 h_\rho} D_\theta \left[\frac{1}{h_\phi}\right] D_\phi \tag{D.4}$$

$$[E_2, E_2] = 0 \tag{D.5}$$

$$[E_2, E_3] = \frac{1}{h_\theta} D_\theta \left[\frac{1}{h_\phi}\right] D_\phi \tag{D.6}$$

$$[E_3, E_3] = 0 \tag{D.7}$$

After substitution, these expressions simplify to

$$[E_1, E_2] = \frac{D_\theta[h_\rho]}{h_\rho^2 h_\theta} D_\rho + \left(-\frac{D_\rho[h_\theta]}{h_\rho h_\theta^2} + \frac{h_\theta h_\rho D_\theta[h_{\rho\theta}] - 2h_{\rho\theta} h_\rho D_\theta[h_\theta] - h_{\rho\theta} h_\theta D_\theta[h_\rho]}{h_\theta^4 h_\rho^2} + \frac{h_{\rho\theta} D_\theta[h_\theta]}{h_\theta^4 h_\rho}\right) D_\theta \tag{D.8}$$

$$[E_1, E_3] = \frac{h_{\rho\theta} D_\theta[h_\phi] - h_\theta^2 D_\rho[h_\phi]}{h_\theta^2 h_\rho h_\phi^2} D_\phi \tag{D.9}$$

$$[E_2, E_3] = -\frac{D_\theta[h_\phi]}{h_\theta h_\phi^2} D_\phi \tag{D.10}$$

With further simplification, we arrive at

$$
\begin{aligned}
[E_1, E_2] =& \frac{D_\theta[h_\rho]}{h_\rho^2 h_\theta} D_\rho \\
&+ \left(\frac{D_\theta[h_{\rho\theta}]}{h_\theta^3 h_\rho} - \frac{h_{\rho\theta} D_\theta[h_\theta]}{h_\theta^4 h_\rho} - \frac{h_{\rho\theta} D_\theta[h_\rho]}{h_\theta^3 h_\rho^2} - \frac{D_\rho[h_\theta]}{h_\rho h_\theta^2} \right) D_\theta \qquad \text{(D.11)} \\
[E_1, E_3] =& \frac{h_{\rho\theta} D_\theta[h_\phi] - h_\theta^2 D_\rho[h_\phi]}{h_\theta^2 h_\rho h_\phi^2} D_\phi \qquad \text{(D.12)} \\
[E_2, E_3] =& - \frac{D_\theta[h_\phi]}{h_\theta h_\phi^2} D_\phi \qquad \text{(D.13)}
\end{aligned}
$$

Plugging the brackets into the metric tensor, we obtain the following non-zero terms:

$$
\begin{aligned}
\langle E_1, [E_1, E_2] \rangle =& \frac{D_\theta[h_\rho]}{h_\rho h_\theta} \qquad \text{(D.14)} \\
\langle E_2, [E_1, E_2] \rangle =& \frac{D_\theta[h_{\rho\theta}]}{h_\theta^2 h_\rho} - \frac{h_{\rho\theta} D_\theta[h_\theta]}{h_\theta^3 h_\rho} - \frac{D_\rho[h_\theta]}{h_\rho h_\theta} \qquad \text{(D.15)} \\
\langle E_3, [E_1, E_3] \rangle =& \frac{h_{\rho\theta} D_\theta[h_\phi] - h_\theta^2 D_\rho[h_\phi]}{h_\theta^2 h_\rho h_\phi} \qquad \text{(D.16)} \\
\langle E_3, [E_2, E_3] \rangle =& - \frac{D_\theta[h_\phi]}{h_\theta h_\phi} \qquad \text{(D.17)}
\end{aligned}
$$

We have that our basis vectors are orthonormal, i.e. $\langle E_i, E_j \rangle = \delta_{i,j}$. Another way of viewing this is that we are using the exponential map to define a locally flat coordinate system [56]. This simplifies Equation D.1 for basis vectors

$$
\langle Z, \nabla_Y X \rangle = -\frac{1}{2} \left(\langle [X, Z], Y \rangle + \langle [Y, Z], X \rangle + \langle [X, Y], Z \rangle \right) \qquad \text{(D.18)}
$$

We can abbreviate our calculations by adopting the following label for the connection coefficients

$$
\langle E_k, \nabla_{E_i} E_j \rangle \equiv \Gamma_{ij}^k \qquad \text{(D.19)}
$$

There are 27 of these symbols from the three dimensions and the three indices, and there is

no symmetry due to the use of a non-coordinate basis.

$$\Gamma^1_{11} = \Gamma^2_{22} = \Gamma^3_{33} = \Gamma^1_{23} = \Gamma^1_{32} = \Gamma^2_{13} = \Gamma^2_{31} = \Gamma^3_{12} = \Gamma^3_{21} = \Gamma^3_{11} = \Gamma^3_{22} = \Gamma^1_{13} = \Gamma^1_{31} = \Gamma^2_{32} = \Gamma^2_{23} = 0 \quad \text{(D.20)}$$

$$\Gamma^2_{11} = -\frac{D_\theta[h_\rho]}{h_\rho h_\theta} \quad \text{(D.21)}$$

$$\Gamma^1_{12} = \frac{D_\theta[h_\rho]}{h_\rho h_\theta} \quad \text{(D.22)}$$

$$\Gamma^2_{12} = 0 \quad \text{(D.23)}$$

$$\Gamma^1_{21} = 0 \quad \text{(D.24)}$$

$$\Gamma^2_{21} = -\left(\frac{D_\theta[h_{\rho\theta}]}{h^2_\theta h_\rho} - \frac{h_{\rho\theta} D_\theta[h_\theta]}{h^3_\theta h_\rho} - \frac{D_\rho[h_\theta]}{h_\rho h_\theta}\right) \quad \text{(D.25)}$$

$$\Gamma^1_{22} = \frac{D_\theta[h_{\rho\theta}]}{h^2_\theta h_\rho} - \frac{h_{\rho\theta} D_\theta[h_\theta]}{h^3_\theta h_\rho} - \frac{D_\rho[h_\theta]}{h_\rho h_\theta} \quad \text{(D.26)}$$

$$\Gamma^1_{33} = \frac{h_{\rho\theta} D_\theta[h_\phi] - h^2_\theta D_\rho[h_\phi]}{h^2_\theta h_\rho h_\phi} \quad \text{(D.27)}$$

$$\Gamma^2_{33} = -\frac{D_\theta[h_\phi]}{h_\theta h_\phi} \quad \text{(D.28)}$$

$$\Gamma^3_{13} = 0 \quad \text{(D.29)}$$

$$\Gamma^3_{31} = -\frac{h_{\rho\theta} D_\theta[h_\phi] - h_\theta^2 D_\rho[h_\phi]}{h_\theta^2 h_\rho h_\phi} \tag{D.30}$$

$$\Gamma^3_{23} = 0 \tag{D.31}$$

$$\Gamma^3_{32} = \frac{D_\theta[h_\phi]}{h_\theta h_\phi} \tag{D.32}$$

So there are eight non-zero "Christoffel" symbols. In order to perform more advanced calculations such as curl, we use the differential forms form of the operations.

REFERENCES

[1] W. Stacey Jr, A. Bailey, D. Sigmar, and K. Shaing, "Rotation and impurity transport in a tokamak plasma with directed neutral-beam injection," *Nuclear fusion*, vol. 25, no. 4, p. 463, 1985.

[2] W. Stacey Jr and D. J. Sigmar, "Viscous effects in a collisional tokamak plasma with strong rotation," *The Physics of fluids*, vol. 28, no. 9, pp. 2800–2807, 1985.

[3] W. M. Stacey and D. Jackson, "Poloidal rotation, density asymmetries, and momentum confinement in tokamak experiments," *Physics of Fluids B: Plasma Physics*, vol. 5, no. 6, pp. 1828–1835, 1993.

[4] W. M. Stacey, "Rotation velocities and radial electric field in the plasma edge," *Contributions to Plasma Physics*, vol. 46, no. 7-9, pp. 597–603, 2006.

[5] W. M. Stacey, R. Johnson, and J. Mandrekas, "A neoclassical calculation of toroidal rotation profiles and comparison with diii-d measurements," *Physics of plasmas*, vol. 13, no. 6, p. 062 508, 2006.

[6] C Bae, W. M. Stacey, and W. M. Solomon, "Extension of neoclassical rotation theory for tokamaks to realistically account for the geometry of magnetic flux surfaces," *Nuclear Fusion*, vol. 53, no. 4, p. 043 011, 2013.

[7] C. Bae, W. M. Stacey, and T. D. Morley, "GTROTA: A code for the solution of the coupled nonlinear extended neoclassical rotation equations in tokamak plasmas using successive over-relaxation and simulated annealing," *Computer Physics Communications*, vol. 184, pp. 2571–2587, Nov. 2013.

[8] W. M. Stacey and B. A. Grierson, "Interpretation of rotation and momentum transport in the diii-d edge plasma and comparison with neoclassical theory," *Nuclear Fusion*, vol. 54, no. 7, p. 073 021, 2014.

[9] T. Collart and W. Stacey, "Improved analytical flux surface representation and calculation models for poloidal asymmetries," *Physics of Plasmas*, vol. 23, no. 5, p. 052 505, 2016.

[10] W. M. Stacey, *Fusion Plasma Physics*, 2nd ed. Wiley-VCH, Oct. 2012, ISBN: 9783527411344.

[11] K. S, *Introductory Nuclear Physics*. Wiley India, 2008, ISBN: 9788126517855.

[12] V. D. Shafranov, B. Bondarenko, G. A. Goncharov, O. A. Lavrentev, A. D. Sakharov, *et al.*, "On the history of the research into controlled thermonuclear fusion," *Physics-Uspekhi*, vol. 44, no. 8, pp. 835–843, 2001.

[13] S. A. Lazerson and J. C. Schmitt, "From tokamaks to stellarators: Understanding the role of 3d shaping," *arXiv preprint arXiv:1705.00517*, 2017.

[14] K Ida and J. Rice, "Rotation and momentum transport in tokamaks and helical systems," *Nuclear Fusion*, vol. 54, no. 4, p. 045 001, 2014.

[15] S. I. Braginskii, "Transport processes in a plasma," *Reviews of plasma physics*, vol. 1, p. 205, 1965.

[16] K. Shaing, K. Ida, and S. Sabbagh, "Neoclassical plasma viscosity and transport processes in non-axisymmetric tori," *Nuclear Fusion*, vol. 55, no. 12, p. 125 001, 2015.

[17] F. Hinton and R. Hazeltine, "Theory of plasma transport in toroidal confinement systems," *Reviews of Modern Physics*, vol. 48, no. 2, p. 239, 1976.

[18] R. Miller, M. Chu, J. Greene, Y. Lin-Liu, and R. Waltz, "Noncircular, finite aspect ratio, local equilibrium model," *Physics of Plasmas*, vol. 5, no. 4, pp. 973–978, 1998.

[19] W. M. Stacey and C. Bae, "Representation of the plasma fluid equations in miller equilibriumi analytical flux surface geometry," *Physics of Plasmas*, vol. 16, no. 8, p. 082 501, 2009.

[20] J. D. Callen, "Anomalous transport in tokamaks: Transport task force reviews," *Physics of fluids B : Plasma physics*, vol. 2, no. 12, pp. 2869–2869, 1990.

[21] F. L. Hinton and S. K. Wong, "Neoclassical ion transport in rotating axisymmetric plasmas," *The Physics of Fluids*, vol. 28, no. 10, pp. 3082–3098, 1985. eprint: `https://aip.scitation.org/doi/pdf/10.1063/1.865350`.

[22] M. N. Rosenbluth, W. M. MacDonald, and D. L. Judd, "Fokker-planck equation for an inverse-square force," *Phys. Rev.*, vol. 107, pp. 1–6, 1 Jul. 1957.

[23] R. D. Hazeltine, "Recursive derivation of drift-kinetic equation," *Plasma Physics*, vol. 15, no. 1, p. 77, 1973.

[24] S. I. Braginskii, "Transport phenomena in a completely ionized two-temperature plasma," *Sov. Phys. JETP*, vol. 6, no. 33, pp. 358–369, 1958.

[25] P. J. Catto and A. N. Simakov, "A drift ordered short mean free path description for magnetized plasma allowing strong spatial anisotropy," *Physics of Plasmas*, vol. 11, no. 1, pp. 90–102, 2004. eprint: https://doi.org/10.1063/1.1632496.

[26] S. Hirshman and D. Sigmar, "Neoclassical transport of impurities in tokamak plasmas," *Nuclear Fusion*, vol. 21, no. 9, p. 1079, 1981.

[27] L. E. Malvern, *Introduction to the Mechanics of a Continuous Medium*, Monograph. 1969.

[28] R. Fitzpatrick, *Plasma physics: an introduction*. Crc Press, 2014.

[29] D. Lovelock and H. Rund, *Tensors, Differential Forms, and Variational Principles*. Dover, 1989, ISBN: 978-0-486-65840-7.

[30] The Numerical Algorithms Group (NAG), *The NAG Library*, Oxford, United Kingdom www.nag.com.

[31] A. H. Glasser, C. R. Sovinec, R. A. Nebel, T. A. Gianakon, S. J. Plimpton, M. S. Chu, D. D. Schnack, and the NIMROD Team, "The nimrod code: A new approach to numerical plasma physics," *Plasma Physics and Controlled Fusion*, vol. 41, no. 3A, A747, 1999.

[32] P. Lax and B. Wendroff, "Systems of conservation laws," *Communications on Pure and Applied mathematics*, vol. 13, no. 2, pp. 217–237, 1960.

[33] S. K. Godunov, "A difference method for numerical calculation of discontinuous solutions of the equations of hydrodynamics," *Matematicheskii Sbornik*, vol. 89, no. 3, pp. 271–306, 1959.

[34] P. D. Lax, "Weak solutions of nonlinear hyperbolic equations and their numerical computation," *Communications on pure and applied mathematics*, vol. 7, no. 1, pp. 159–193, 1954.

[35] B. P. Leonard, "A stable and accurate convective modelling procedure based on quadratic upstream interpolation," *Computer methods in applied mechanics and engineering*, vol. 19, no. 1, pp. 59–98, 1979.

[36] J. VonNeumann and R. D. Richtmyer, "A method for the numerical calculation of hydrodynamic shocks," *Journal of applied physics*, vol. 21, no. 3, pp. 232–237, 1950.

[37] D. D. Schnack, D. C. Barnes, D. P. Brennan, C. C. Hegna, E Held, C. C. Kim, S. E. Kruger, A. Y. Pankin, and C. R. Sovinec, "Computational modeling of fully ionized magnetized plasmas using the fluid approximation," *Physics of plasmas*, vol. 13, no. 5, p. 058 103, 2006.

[38] N. Ferraro and S. C. Jardin, "Finite element implementation of braginskiis gyroviscous stress with application to the gravitational instability," *Physics of plasmas*, vol. 13, no. 9, p. 092 101, 2006.

[39] E. Howell and C. Sovinec, "Solving the gradshafranov equation with spectral elements," *Computer Physics Communications*, vol. 185, no. 5, pp. 1415 –1421, 2014.

[40] A. N. Brooks and T. J. Hughes, "Streamline upwind/petrov-galerkin formulations for convection dominated flows with particular emphasis on the incompressible navier-stokes equations," *Computer methods in applied mechanics and engineering*, vol. 32, no. 1-3, pp. 199–259, 1982.

[41] K. A. Croft and T. M. Moeller, "Implementation of a supg stabilized finite element method for a two fluid plasma model," in *2018 Plasmadynamics and Lasers Conference*, 2018, p. 2942.

[42] J. V. Gutiérrez-Santacreu, O. Maj, and M. Restelli, "Finite element discretization of a stokes-like model arising in plasma physics," *Journal of Computational Physics*, vol. 373, pp. 811–834, 2018.

[43] C. Sovinec, A. Glasser, T. Gianakon, D. Barnes, R. Nebel, S. Kruger, S. Plimpton, A. Tarditi, M. Chu, and the NIMROD Team, "Nonlinear magnetohydrodynamics with high-order finite elements," *J. Comp. Phys.*, vol. 195, p. 355, 2004.

[44] T. Warburton and G. Karniadakis, "A discontinuous galerkin method for the viscous mhd equations," *Journal of computational Physics*, vol. 152, no. 2, pp. 608–641, 1999.

[45] Wolfram Research, Inc., *Mathematica, Version 11.3*, Champaign, IL, 2018.

[46] R. Courant, K. Friedrichs, and H. Lewy, "Über die partiellen differenzengleichungen der mathematischen physik," *Mathematische annalen*, vol. 100, no. 1, pp. 32–74, 1928.

[47] D. A. Knoll and D. E. Keyes, "Jacobian-free newton–krylov methods: A survey of approaches and applications," *Journal of Computational Physics*, vol. 193, no. 2, pp. 357–397, 2004.

[48] W. Stacey and C Bae, "Extension of the flow-rate-of-strain tensor formulation of plasma rotation theory to non-axisymmetric tokamaks," *Physics of Plasmas*, vol. 22, no. 6, p. 062 503, 2015.

[49] J. T. Grétarsson and R. Fedkiw, "Fully conservative leak-proof treatment of thin solid structures immersed in compressible fluids," *Journal of Computational Physics*, vol. 245, pp. 160–204, 2013.

[50] K. H. Burrell, W. W. Heidbrink, M. J. Lanctot, N. A. Pablant, B. A. Grierson, and W. M. Solomon, "Measurements of the deuterium ion toroidal rotation in the diii-d tokamak and comparison to neoclassical theory," *Physics of plasmas*, vol. 19, no. 5, 2012.

[51] B. Lipschultz, P. J. Catto, R. M. McDermott, M. L. Reinke, K. D. Marr, B Lipschultz, P. J. Catto, R. M. McDermott, M. L. Reinke, and A. N. Simakov, "Comparison of neoclassical predictions with measured flows and evaluation of a poloidal impurity density asymmetry," *Plasma physics and controlled fusion*, vol. 52, no. 5, 2010.

[52] R. G. J. Cramp, S. Gibson, S. A. Lazerson, I. T. Chapman, C. Ham, and A Kirk, "Non-axisymmetric ideal equilibrium and stability of iter plasmas with rotating rmps," *Nuclear fusion*, vol. 56, no. 8, 2016.

[53] J. P. Boyd, *Chebyshev and Fourier spectral methods*. Courier Corporation, 2001.

[54] L. C. Evans, *Partial differential equations*. Providence, R.I.: American Mathematical Society, 2010, ISBN: 9780821849743.

[55] H. Grad and H. Rubin, "Hydromagnetic equilibria and force-free fields," *Journal of Nuclear Energy (1954)*, vol. 7, no. 3-4, pp. 284–285, Oct. 1958.

[56] M. do Carmo, *Riemannian Geometry*, ser. Mathematics (Boston, Mass.) Birkhäuser, 1992, ISBN: 9783764334901.